HHS Public Access

Author manuscript

Sci Immunol. Author manuscript; available in PMC 2024 April 23.

Published in final edited form as:

Sci Immunol. 2022 February 11; 7(68): eabi6763. doi:10.1126/sciimmunol.abi6763.

Protein kinase R is an innate immune sensor of proteotoxic stress via accumulation of cytoplasmic IL-24

Sophia Davidson[1,2], **Chien-Hsiung Yu**[1,2], **Annemarie Steiner**[1,2,3], **Frédéric Ebstein**[4], **Paul J. Baker**[5], **Valentina Jarur-Chamy**[6], **Katja Hrovat Schaale**[1], **Pawat Laohamonthonkul**[1], **Klara Kong**[1], **Dale J. Calleja**[7], **Cassandra R. Harapas**[1,2], **Katherine R. Balka**[8], **Jacob Mitchell**[9], **Jacob T. Jackson**[10], **Niall D. Geoghegan**[11], **Fiona Moghaddas**[1,2], **Kelly L. Rogers**[11], **Katrin D. Mayer-Barber**[5], **Adriana A. De Jesus**[9], **Dominic De Nardo**[8], **Benjamin T. Kile**[8,12], **Anthony J. Sadler**[13,14], **M. Cecilia Poli**[6,15], **Elke Krüger**[4], **Raphaela Goldbach Mansky**[9], **Seth L. Masters**[1,2,*]

[1]Inflammation Division, Walter and Eliza Hall Institute of Medical Research, Parkville, Victoria 3052, Australia.

[2]Department of Medical Biology, University of Melbourne, Parkville, Victoria 3010, Australia.

[3]Institute of Structural Biology, University Hospital Bonn, Bonn 53127, Germany.

[4]University Medicine Greifswald, Institute of Medical Biochemistry and Molecular Biology, Greifswald 17475, Germany.

[5]Inflammation and Innate Immunity Unit, Laboratory of Clinical Immunology and Microbiology, NIAID, NIH, Bethesda, MD 20892, USA.

[6]Immunogenetics and Translational Immunology Program. Facultad de Medicina, Universidad del Desarrollo Clínica Alemana, Santiago, Chile.

[7]Ubiquitin Division, Walter and Eliza Hall Institute of Medical Research, Parkville, Victoria 3052, Australia.

[8]Department of Anatomy and Developmental Biology, Monash Biomedicine Discovery Institute, Monash University, Clayton, Victoria, Australia.

[9]Translational Autoinflammatory Disease Studies (TADS), Laboratory of Clinical Immunology and Microbiology, NIAID, NIH, Bethesda, MD 20892, USA.

[*]Corresponding author. masters@wehi.edu.au.

Author contributions: S.D. and S.L.M conceived the study, designed the experiments, and wrote the original draft of the manuscript. S.D., C.-H.Y., A.S., F.E., P.J.B., V.J.-C., K.H.S., P.L., K.K., D.J.C., C.R.H., K.R.B., J.M., J.T.J., N.D.G., and A.A.D.J. performed experiments. F.M., K.L.R., K.D.M.-B., D.D.N., B.T.K., A.J.S., M.C.P., E.K., and R.G.M. made important conceptual contributions. All authors contributed to the final manuscript.

Competing interests: The authors declare that they have no competing interests.

SUPPLEMENTARY MATERIALS

www.science.org/doi/10.1126/sciimmunol.abi6763

Figs. S1 to S4

Tables S1 to S5

Movies S1 and S2

View/request a protocol for this paper from Bio-protocol.

[10]Immunology Division, Walter and Eliza Hall Institute of Medical Research, Parkville, Victoria 3052, Australia.

[11]Centre for Dynamic Imaging, Walter and Eliza Hall Institute of Medical Research, Parkville, Victoria 3052, Australia.

[12]Faculty of Health and Medical Sciences, University of Adelaide, Adelaide, South Australia 5000, Australia.

[13]Centre for Innate Immunity and Infectious Diseases, Hudson Institute of Medical Research, Clayton, Victoria, Australia.

[14]Department of Molecular and Translational Sciences, Monash University, Clayton, Victoria, Australia.

[15]Division of Pediatric Immunology, Allergy, and Rheumatology, Department of Pediatrics, Baylor College of Medicine, Houston, TX 77030, USA.

Abstract

Proteasome dysfunction can lead to autoinflammatory disease associated with elevated type I interferon (IFN-αβ) and NF-κB signaling; however, the innate immune pathway driving this is currently unknown. Here, we identified protein kinase R (PKR) as an innate immune sensor for proteotoxic stress. PKR activation was observed in cellular models of decreased proteasome function and in multiple cell types from patients with proteasome-associated autoinflammatory disease (PRAAS). Furthermore, genetic deletion or small-molecule inhibition of PKR in vitro ameliorated inflammation driven by proteasome deficiency. In vivo, proteasome inhibitor–induced inflammatory gene transcription was blunted in PKR-deficient mice compared with littermate controls. PKR also acted as a rheostat for proteotoxic stress by triggering phosphorylation of eIF2α, which can prevent the translation of new proteins to restore homeostasis. Although traditionally known as a sensor of RNA, under conditions of proteasome dysfunction, PKR sensed the cytoplasmic accumulation of a known interactor, interleukin-24 (IL-24). When misfolded IL-24 egress into the cytosol was blocked by inhibition of the endoplasmic reticulum–associated degradation pathway, PKR activation and subsequent inflammatory signaling were blunted. Cytokines such as IL-24 are normally secreted from cells; therefore, cytoplasmic accumulation of IL-24 represents an internal danger-associated molecular pattern. Thus, we have identified a mechanism by which proteotoxic stress is detected, causing inflammation observed in the disease PRAAS.

INTRODUCTION

Monogenic autoinflammatory diseases are characterized by systemic and organ-specific inflammation resulting from dysregulation of the innate immune system (1). Proteasome-associated autoinflammatory syndrome (PRAAS) is a spectrum of autoinflammatory disease driven by autosomal recessive homozygous, compound heterozygous, or dominant negative loss-of-function mutations in genes coding for proteasome subunits or the proteasome maturation protein (POMP). This includes loss-of-function mutations in the genes *PSMB8* and *PSMB9*, which encode inducible proteasome subunits iβ5 and iβ1, respectively,

of the immunoproteasome complex (2–8). These patients suffer a severe inflammatory disease involving joint contractures, muscle atrophy, microcytic anemia, chronic atypical neutrophilic dermatosis with lipodystrophy, and elevated temperature (3).

The proteasome is expressed in all eukaryote cells and functions to degrade unwanted proteins tagged with ubiquitin. This includes proteins that are terminally misfolded and ejected from the endoplasmic reticulum (ER) via the ER-associated degradation (ERAD) pathway. In this way, the ubiquitin proteasome system (UPS) protects the cell from buildup of unwanted proteins (proteotoxic stress) and maintains cellular homeostasis. Aggregates of ubiquitinated proteins are observed in PRAAS patient cells, and this loss of proteostasis is associated with an interferon-stimulated gene (ISG) signature and elevated proinflammatory cytokines in patient blood (2, 3, 5, 6). Blockade of this inflammatory signaling using Janus kinase inhibitors is an effective treatment for patients with PRAAS (9), demonstrating that the central role inflammation plays in PRAAS pathogenesis. Despite this, it is currently unknown whether there is a specific cytosolic sensor for proteotoxic stress to trigger this inflammatory response.

Here, we used a cellular model for PRAAS and identifed protein kinase R (PKR) as the innate immune sensor activated by proteasome dysfunction. PKR was not activated by its canonical ligand, double-stranded RNA but instead bound to the cytokine interleukin-24 (IL-24). Accumulation of misfolded IL-24 in the cytosol occurred when the proteasome failed to clear it from the cytoplasm. Being a cytokine, IL-24 should be secreted directly from the cell, so this accumulation suggested that IL-24 could be a danger-associated molecular pattern (DAMP), hence the initiation of a PKR-driven inflammatory response. This study identified an innate inflammatory cascade resulting from proteotoxic stress.

RESULTS

Generation of PRAAS model cell lines

We generated an in vitro model of PRAAS using inducible CRISPR- Cas9–mediated genetic deletions of the immunoproteasome subunits iβ5 and iβ1 in THP-1 cells, a human monocytic cell line (Fig. 1A). iβ5 and iβ1 were efficiently deleted in THP-1 cell pools using multiple single guide RNAs (table S1). We also observed a decrease in iβ1 levels in $i\beta5^{-/-}$ cells because iβ5 is required for the maturation of and incorporation of iβ1 into the immunoproteasome (10). Our PRAAS model cell lines recapitulated the accumulation of high–molecular weight ubiquitin-conjugated protein species (Fig. 1A) and confirmed the critical role of the immunoproteasome in preserving protein homeostasis (11). Moreover, these PRAAS model cell lines exhibited a similar inflammatory profile as that observed in PRAAS patients with increased transcription and secretion of interferon-β (IFN-β) (Fig. 1, B and D) and elevated levels of IFN-α protein as observed at a single-cell level via flow cytometry (Fig. 1C). Consistent with elevated IFN-αβ secretion in PRAAS model cell lines, we observed increased activation of the IFN-αβ downstream signaling molecule signal transducer and activator of transcription 1 (STAT1) by flow cytometry (Fig. 1C). Elevated STAT1 phosphorylation was indicative of increased STAT1 signaling in these cells and not the result of significant changes in total STAT1 levels as a whole (fig. S1A). In addition, secretion of the IFN-αβ–inducible chemokine C-X-C motif chemokine 10 (CXCL10) and

gene transcription of the ISGs MX dynamin-like guanosine triphosphatase 1 (*MX1*) and ISG15 ubiquitin-like modifier (*ISG15*) were all elevated in PRAAS model cells (Fig. 1, B and D). We also observed activation of nuclear factor κB (NF-κB) signaling in PRAAS model cell lines at baseline by immunoblot (Fig. 1A), and increased gene expression of NF-κB– induced cytokines *IL6* and *TNF* was observed via quantitative polymerase chain reaction (qPCR) (Fig. 1D).

Consistent with the inflammatory phenotype of the cell line being due to an accumulation of ubiquitinated species targeted for proteasomal degradation, a broad-spectrum deubiquitinase (DUB) inhibitor PR619 markedly increased this proteotoxic stress and the resulting inflammatory gene expression (Fig. 1D). As an independent confirmation, pharmacological proteasome inhibitors were examined, including oprozomib, which inhibits both the β5 and iβ5 proteasomal subunits (12). Treatment of THP-1 cells with oprozomib induced *IFNB1* mRNA to levels similar to basal expression in $i\beta5^{-/-}$ cells, and combining these had no additional effect, indicating that both approaches were likely to be on target (fig. S1B). Thus, our CRISPR-Cas9–generated cell lines recapitulated the central PRAAS phenotypes necessary to investigate the innate immune responses to proteotoxic stress.

Proteotoxic stress activates PKR

Our $i\beta5^{-/-}$ and $i\beta1^{-/-}$ cell lines confirmed findings from patients with PRAAS that the innate immune response to proteotoxic stress involved activation of both IFN-αβ and NF-κB signaling pathways. Because there are several candidate innate immune sensors that are capable of triggering both of these pathways, we took a hypothesis-driven approach to study each in turn. To begin, we generated cells deficient in Unc-93 homolog B1 (UNC93B1) (fig. S2A), because it is essential for signaling downstream of multiple Toll-like receptors (TLRs) (TLR3, TLR5, TLR7, TLR8, and TLR9) (13). However, treatment with the β1/β5 proteasome inhibitor delanzomib (14) or oprozomib did not alter transcription of inflammatory genes such as *IFNB1* in UNC93B1-deficient human THP-1 cells (Fig. 2A and fig. S2B), and we observed similar results in $Unc93b1^{-/-}$ mouse bone marrow–derived macrophages (fig. S2C). We next generated THP-1 cells deficient in mitochondrial antiviral signaling (MAVS) protein, which controls inflammatory signaling from retinoic acid-inducible gene-I and melanoma differentiation-associated protein 5 (MDA-5) (15) and stimulator of interferon genes (STING), which regulates signaling downstream of cyclic GMP–AMP synthase (cGAS) (fig. S2D) (15). Mouse embryonic fibroblasts (MEFs) and human THP-1 cell lines deficient in either MAVS or STING showed no impediment of *IFNB1* or other inflammatory gene induction upon treatment with oprozomib or delanzomib (Fig. 2B and fig. S2E). In notable contrast, THP-1 cells and MEFs deficient in PKR exhibited no increase in *IFNB1* mRNA expression upon chemical inhibition of the proteasome (Fig. 2, B and C). Confirmation of PKR deletion is shown by Western blot in Fig. 2D. Similarly, induction of NF-κB– driven inflammatory gene *IL6* was also abrogated in PKR-deficient THP-1 cells (fig. S2E). PKR drives the induction of IFN-αβ via tumor necrosis factor (TNF) receptor–associated factor 3 (TRAF3) (16, 17) and NF-κB activation through a direct interaction with TRAF2 and TRAF5 (18). This abolishment of *IFNB1* gene induction due to PKR deficiency was specific to proteasome inhibition because stimulation of the STING signaling pathway with cyclic guanosine monophosphate–

adenosine monophosphate (cGAMP) induced *IFNB1* transcription to comparable levels between parental and PKR-deficient THP-1 cells (Fig. 2C).

We observed increased activation (phosphorylation) of PKR in both PRAAS model cell lines as compared with parental THP-1 cells (Fig. 2D). Genetic deletion of PKR in PRAAS cell lines resulted in a loss of STAT1 phosphorylation and blunted inflammatory gene expression (Fig. 2, D and E, and fig. S2F). Chemical inhibition of PKR using the specific inhibitor C16 (19) ameliorated the elevated expression of inflammatory genes in $i\beta5^{-/-}$ cells (Fig. 2F and fig. S2G). To complete this analysis, we studied mice deficient in PKR ($PKR^{-/-}$) and their littermate controls ($PKR^{+/+}$). Treatment with the proteasome inhibitor bortezomib induced up-regulation of *Ifnb1*, *Ifna4*, *Il6*, and *Usp18* mRNA in $PKR^{+/+}$ blood and splenic samples 18 hours after intraperitoneal injection. However, deficiency in PKR blunted bortezomib-driven inflammatory gene transcription in both the blood and spleen (Fig. 2G and fig. S2H). These data demonstrated that PKR is an innate immune sensor for inflammation downstream of proteasome inhibition both in vitro and in vivo.

Activation of PKR in a disease driven by proteasome dysfunction is particularly noteworthy, as PKR is part of a family of kinases that phosphorylate eukaryotic initiation factor 2 on its α-subunit (eIF2α) (20). eIF2α functions to repress protein translation; thus, PKR-mediated activation of eIF2α will reduce the proteotoxic burden on the cell as a negative feedback mechanism, likely restoring the cell to homeostasis. We observed increased phosphorylation of eIF2α in PRAAS model cells (Fig. 2D). Genetic deletion of the three other eIF2α kinase family members [heme-regulated inhibitor (HRI), PKR-like ER kinase (PERK), or general control nonderepressible 2 (GCN2)] (fig. S2D) had no impact on delanzomib-induced inflammatory gene transcription, suggesting that they were not required or were redundant with PKR for this process (fig. S2E).

PKR is activated by IL-24

Having identified PKR as a pattern recognition receptor (PRR) activated under conditions of proteasome dysfunction, we next wanted to determine exactly how PKR was being activated. Typically, PKR functions as a sensor of cytoplasmic double-stranded viral RNA (21, 22). Recently, it has been suggested that PKR can also be triggered endogenously by mitochondrial RNA (23). To test this, we created mitochondrial DNA (mtDNA)–depleted THP-1 cells (ρ^0 cells) by culturing with low-dose ethidium bromide to achieve a mitochondrial transcript-free condition (24). Depletion was confirmed by decreased expression of mitochondrial genes (*MT-ND1*, *MT-ND2*, and *MT-ND3*), determined by qPCR and changes in the mtDNA binding protein, transcription factor A, mitochondrial (TFAM), as assessed by immunoblot (fig. S2, H and I). When these cells were treated with proteasome inhibitors, the induction of *IFNB1* and *IL6* was comparable between untreated cells and ρ^0 cells (fig. S2K), indicating that the DAMP that triggers PKR during proteotoxic stress is unlikely to be mitochondrial RNA.

PRAAS is characterized by the accumulation of unwanted proteins in the cell, so we next interrogated known protein activators of PKR, which include protein activator of PKR (PACT) (25), trans-activation response element RNA-binding protein (TRBP) (26), and the cytokine IL-24 (also known as MDA-7) (27). We hypothesized that accumulation of one of

these known interactors of PKR due to decreased proteasome activity could act as a DAMP and activate PKR. To test this, we performed genetic deletion of each of the aforementioned interactors from THP-1 cells (fig. S3A), revealing that IL-24 was the only candidate required for induction of inflammation in response to the proteasome inhibitor delanzomib (Fig. 3A). This decreased *IFNB1* mRNA induction in IL-24$^{-/-}$ cells was specific to proteasome inhibition, because stimulation of the cGAS signaling pathway with poly(dA:dT)-induced *IFNB1* transcription to the same extent as what was observed in parental THP-1 cells (Fig. 3A). Consistent with our hypothesis, we observed a higher level of IL-24 in our PRAAS model cell lines by flow cytometry analysis (fig. S3B). CRISPR-Cas9 deletion of IL-24 from PRAAS model cell lines blunted inflammatory gene induction, as assessed by qPCR (Fig. 3B and fig. S3C). Activation of PKR and consequent phosphorylation of STAT1 and eIF2α were also reduced in both iβ5$^{-/-}$ and iβ1$^{-/-}$ cell lines deficient in IL-24, as assessed by immunoblot (Fig. 3c). Induction of *IFNB1* and other inflammatory genes could be restored when IL-24 was exogenously expressed in IL-24$^{-/-}$ cells (fig. S3A), and this was dependent on the presence of PKR (Fig. 3D and fig. S3D). To confirm these observations in vivo, we injected control mice or IL-24$^{-/-}$ mice with bortezomib and performed immunoblot on protein lysates generated from spleens for (p)eIF2α and (p)STAT1. The phosphorylation of these factors occurs downstream of PKR and was induced by proteasome inhibition in control mice but not in IL-24$^{-/-}$ mice (fig. S3E). Collectively, these data indicated that in proteasome-defective cell lines and in a mouse model of proteasome inhibition, IL-24 drives PKR-dependent inflammation.

IL-24 is a secreted cytokine and signals via cell surface receptor complexes that all include IL-20RB (28). Genetic deletion of the IL-20RB receptor subunit was performed in THP-1 cells, although the expression of the gene is reported to be negligible in this cell line (29), so validation by Western blot was not possible. Nevertheless, there was no effect on proteasome inhibitor–triggered *IFNB1* or *IL6* transcription, suggesting that the effect of IL-24 was not due to extracellular signaling events (Fig. 3E). These data, along with previous reports (27, 30), indicated that IL-24 was likely interacting directly with PKR as a result of intracellular accumulation after proteasome inhibition.

Under conditions of proteasome dysfunction IL-24 accumulates in the cytosol

To determine whether PKR and IL-24 were interacting under conditions of proteasome dysfunction, we performed an immunoprecipitation (IP) of PKR in iβ5$^{-/-}$ THP-1 cells versus control lines. IL-24 was immunoprecipitated in complex with PKR, and this only occurred when the proteasome was disrupted (Fig. 3F). The band corresponding to IL-24 in the whole-cell lysate (WCL) is a broadsize range, whereas the species immunoprecipitated by PKR correspond to the lower molecular weights of this range. One potential explanation for this is that IL-24 encounters *N*-glycanase in the cytosol, and deglycosylation of IL-24 by *N*-glycanase would reduce the molecular weight of the cytokine (31). To investigate this further, we generated a mutant IL-24 construct (IL-24$^{N86Q, N99Q, N126Q}$), which could not be glycosylated, and found this species of IL-24 migrated with a significantly reduced size compared with wild-type IL-24 (fig. S3F). To compare the size of IL-24 species recovered by PKR-IP with the size of deglycosylated IL-24, we treated WCLs of iβ5$^{-/-}$ stably expressing IL-24 cells with the endoglycosidase peptide *N*-glycosidase F (PNGase

F) to remove N-linked glycans (fig. S3G). When compared with WCL IL-24, the species immunoprecipitated by PKR had a higher electrophoretic mobility, similar to that of the PNGase F–treated sample (lanes 6 and 7). We observed two distinct bands of IL-24 in the iβ5$^{-/-}$ PKR-IP sample (lane 6), one at ~25 kDa, which was likely a partially glycosylated form of IL-24, and another at ~18 kDa, which was the predicted size of fully deglycosylated IL-24 (32). These data provided independent evidence that IL-24 interacts with PKR in the cytosol, not when released from the ER after lysis.

To further investigate cytosolic accumulation of IL-24, we created U2OS cells with low, stable expression of IL-24–Halo (fig. S3H) and imaged them by super-resolution microscopy. We detected an accumulation of IL-24 in cells treated with the proteasome inhibitor delanzomib over time. Accumulation of IL-24 occurred both inside the ER, stained with ER-Tracker, and also in the surrounding cytoplasm (Fig. 3, G and H). Furthermore, we imaged the cells in real time by lattice light-sheet microscopy so as to avoid photobleaching over 7 hours. Control cells show no cytosolic IL-24 (movie S1); however, IL-24-Halo greatly accumulates outside of the ER after delanzomib treatment (movie S2). These data demonstrated that IL-24 could escape the ER, and under conditions where the proteasome is inhibited, it accumulates in the cytoplasm.

IL-24 encodes a signal peptide for constitutive secretion via the ER (33). Cytokines that are misfolded exit the ER and enter the cytosol for proteasomal degradation via the ERAD pathway (34). We hypothesized that IL-24 acts as a quality control mechanism for the UPS; if proteasome function is decreased, misfolded IL-24 will accumulate in the cytosol. Accumulating IL-24 levels in the cytosol alert the cell to proteasome dysfunction by activating PKR. Kifunesine is a mannosidase I inhibitor that promotes ER retention of misfolded proteins (35). Consistent with our hypothesis, treatment with kifunesine prevented cytosolic accumulation of IL-24 for U2OS cells and the induction of *IFNB1* and *IL6* for THP-1 cells, in response to proteasome inhibition (Fig. 3, G to I). Similarly, another mannosidase I inhibitor, 1-deoxymannojirimycin hydrochloride (DMJM), also prevented IL-24 accumulation in the cytoplasm and blunted inflammatory gene induction downstream of proteasome inhibition (fig. S3, I and J). In contrast, a mannosidase II inhibitor, Swainsonine (SW), which does not prevent ERAD, did not halt IL-24 cytosolic accumulation or inflammatory gene induction (fig. S3, I and J). The toxicity of kifunesine, DMJM, and SW was ruled out by propidium iodide viability staining of THP-1 cells treated with these inhibitors for 14 hours (fig. S3K). Thus, ERAD inhibition prevented activation of PKR and consequent inflammatory signaling by promoting retention of IL-24 in the ER.

One mechanism by which proteins misfold and are selected for ERAD is insufficient glycosylation. In agreement with this, mutating one or more of the three IL-24 glycosylation sites (N86, N99, and N126) leads to its accumulation in the cytosol (32). Shorter isoforms of IL-24 mRNA have been identified with exons coding for these key glycosylation sites spliced out (36–39). To investigate the relative contribution of these splice isoforms in PRAAS, we performed PCR amplification of IL-24 RNA (36) from PRAAS patient and healthy control (HC) fibroblast lines. All lines expressed full length IL-24 mRNA, whereas smaller isoforms were predominantly observed in PRAAS patient cells, the most prominent of which corresponded to IL-24 ΔEx5. After serum starvation, IL-24 levels, in general,

and IL-24 ΔEx5, specifically, were amplified in PRAAS fibroblasts yet decreased in HC cells (Fig. 3J). Although we did not see a significant amount of IL-24 ΔEx5 protein accumulate in PRAAS samples by immunblot, the overexpressed protein did accumulate more in the cytosol in contrast to full length IL-24 (Fig. 3K). It is also informative that IL-24 ΔEx5 lacks lysine-123 (K123), which is reported as the main ubiquitination site regulating its proteasomal degradation (40). However, IL-24 ΔEx5 accumulation in the cytosol was still enhanced due to proteasome inhibition, which suggested that lysine residues other than K123 can facilitate its ubiquitin-mediated degradation (Fig. 3K). We also performed immunoprecipitation of IL-24 ΔEx5 and confirmed that its interaction with PKR is induced by proteasome deficiency (fig. S3L). Thus, transcriptional regulation of IL-24 isoforms could contribute to PRAAS, although the physiological relevance for this is currently unclear.

PKR drives inflammation in PRAAS samples

Although our studies identified PKR as a sensor of proteotoxic stress due to accumulating cytosolic IL-24, these observations were based on model systems. Therefore, we looked to confirm our results in samples from patients suffering from PRAAS. Fibroblasts and peripheral blood mononuclear cells (PBMCs) from patients with mutations in proteasomal subunits exhibited increased levels of IL-24, phosphorylated PKR, and eIF2α (Fig. 4, A and B). Similarly, patients with loss-of-function mutations in POMP also exhibited elevated levels of PKR phosphorylation (fig. S4A). These patients have since undergone hematopoietic stem cell transplantation, which corrected their immune dysregulation, indicating that proteasome dysfunction in hematopoietic cells is sufficient to drive systemic interferonopathy (41). Significantly, we performed cellular fraction on PRAAS patient and HC fibroblast lines and observed increased levels of IL-24 in both the membrane and cytosolic portions of PRAAS patient samples compared with HCs (fig. S4B). Furthermore, IL-24 was immunoprecipitated by PKR from PRAAS patient fibroblast lysates and not in HC lysates (fig. S4C). These data provided physiological evidence for proteasomal dysfunction leading to an interaction between IL-24 and PKR in the cytoplasm in PRAAS patient cells.

Treatment of PRAAS PBMCs with the PKR inhibitor C16 ablated PKR phosphorylation in patient PBMCs, which led to a decrease in activation of STAT1 and eIF2α in patient cells (Fig. 4B). C16 significantly decreased IFN-αβ and ISG gene expression in PRAAS patient PBMCs (Fig. 4C and fig. S4D). This pathway was specific to PRAAS, as PKR inhibition in PBMC samples from patients suffering from STING-associated vasculopathy with onset in infancy (SAVI), another known interferonopathy, did not alter IFN-αβ subtype or ISG gene expression (Fig. 4C). We also investigated whether activation of other ER stress pathways in PRAAS patient cells were contributing to inflammatory signaling. The small-molecule inhibitor guanabenz binds to a regulatory subunit of protein phosphatase 1 (PPP1R15A, also known as GADD34) and thereby prevents dephosphorylation of eIF2α. This prolonging of eIF2α phosphorylation protects cells from protein misfolding stress (42). We assessed the effect of guanabenz treatment on inflammatory gene transcription on the expanded T cell populations generated from two individual PRAAS patients (PRAAS #4 and #5). Guanabenz treatment did not normalize ISG expression in PRAAS patient samples (fig. S4D). Similarly,

inhibition of the inositol requiring enzyme 1α/β (IRE1) arm of the unfolded protein response using the inhibitor 4μ8C did not alter ISG expression in PRAAS patient T cells (fig. S4D). These data suggested that although unfolded protein response stress pathways are activated in PRAAS patient cells, inhibition of these does not blunt type I IFN signaling. In contrast, treatment of both patients' T cells with the PKR inhibitor C16 decreased ISG expression (fig. S4D). Last, to control for possible environmental variability in clinically isolated samples, we also confirmed our results in patient-derived induced pluripotent stem cells (iPSCs). We differentiated macrophages from PRAAS patient and healthy donor iPSCs. These iPSC lines were kept under identical conditions throughout differentiation and maturation. Concordant with our results from patient PBMCs, we observed elevated IFN-αβ subtype transcription in PRAAS patient-derived cells, which could be normalized using C16 (Fig. 4D). Collectively, these data demonstrated the potential of PKR inhibition as a targeted treatment for proteasome dysfunctional disorders.

DISCUSSION

Innate immune sensing of cytoplasmic RNA and DNA is well characterized; however, mechanisms that sense misfolded or aggregated protein in the cytosol are not well defined. Using PRAAS as a model of accumulation of proteotoxic burden, we identified a PRR that sensed the buildup of unwanted protein in cells. Activation of PKR is also observed in Aicardi-Goutieres syndrome, an interferonopathy that can be caused by loss-of-function mutations in adenosine deaminases acting on RNA (ADAR1). Lack of ADAR1 results in a failure to edit endogenous Alu repeats, resulting in their self-recognition not only by PKR but also MDA-5 (43). Although disease manifestations vary greatly between interferonopathies, multiple innate immune sensors may be triggered, therefore small-molecule inhibition of PKR could be therapeutically beneficial in certain interferonopathies, as we have demonstrated in PRAAS patient cells ex vivo.

Our observation that PKR can be triggered by proteotoxic stress may help to explain the broad array of pathologies associated with PKR activation. These include neurodegenerative diseases associated with an accumulation of unwanted proteins and inflammatory signaling such as Parkinson's and Alzheimer's diseases (44). In animal models of Alzheimer's disease, genetic deletion or chemical inhibition of PKR ameliorated neuroinflammation and cognitive deficits (45–47). On the other hand, driving proteotoxic stress and possible PKR activation through chemical inhibition of the proteasome in certain disease settings, such as multiple myeloma, can be beneficial (48). In this case, pathogenic B cells are depleted because proteasome inhibitors such as bortezomib place additional stress on a malignant cell type that is already struggling to deal with high rates of protein synthesis and degradation. It is intriguing to speculate whether any of the success of these therapies is associated with the mechanism we now describe, given the known anticancer role of IFN-αβ (49). In contrast, proteasome inhibitor therapy has not been successfully adapted to systemic lupus erythematosus (lupus), an autoimmune disease driven by pathogenic plasma cells. Although plasma cell depletion in one study was achieved (50), patients suffered significant adverse events (51), and we suggest that these may be due to activation of PKR-driven inflammation, which would exacerbate pathology in lupus.

PKR detection of proteotoxic stress probably did not evolve to function in these contexts of sterile inflammation. Instead, it is likely that this pathway developed to counteract pathogen invasion; indeed, several human pathogens target the host proteasome (52). In particular, viruses such as HIV-1, hepatitis C virus (HCV), and human cytomegalovirus (HCMV), which establish chronic or persistent infections in humans, all encode factors that interfere with proteasome function, including prevention of transcriptional up-regulation of immunoproteasome components and direct interaction of viral proteins with immunoproteasome and proteasome subunits (53–55). All of the aforementioned viruses have evolved specific mechanisms to inhibit PKR activation or signaling, including coding for competitive binding proteins such as Tat by HIV or PKR-interacting proteins, NS5A and E2 encoded by HCV, and pTRS1 from HCMV (56–59), indicating an intimate and competitive evolutionary relationship. In light of this, we suggest that PKR activation in response to proteasome inhibition by pathogen effectors is likely to be an underappreciated arm of innate immune defense.

PKR detection of proteasomal stress is also an appropriate response to infection because it can return the cell to homeostasis when the pathogen is cleared by phosphorylating eIF2α and reducing de novo protein synthesis. PKR is only one of a family of four kinases that activate eIF2α, including PERK, GCN2, and HRI. All eIF2α kinase family members are implicated in the phosphorylation of eIF2α in response to proteasome inhibition and therefore may also play a role in subsequent regulation of inflammation and resolution of misfolded protein accumulation (60–63). It is intriguing to speculate that there is a conserved role of these kinases to detect and regulate cell proteostatsis. Differences in activation of these kinases may reflect the kind of proteasome being inhibited and the cell type where the inhibition is occurring.

We demonstrated a mechanism by which PKR senses proteotoxic stress via cytoplasmic detection of a cytokine, which should otherwise be secreted from the cell. This is consistent with other innate immune sensors recognizing DNA or RNA outside of mitochondria or the nucleus but represents a paradigm shift for proteins, which are typically not considered as DAMPs in the cytoplasm. Although this finding is unexpected, perhaps there is an as-yet-underappreciated role for intracellular cytokine recognition in innate immunity. In HBV-infected human hepatocytes, presence of the cytokine IL-32 in the cytosol activates extracellular signal–regulated kinase 1/2 signaling and thereby inhibits viral replication (64). Furthermore, there is a series of virally encoded molecules that resemble cytokines, so-called virokines, including one that resembles IL-24 made by a poxvirus (65). Whether this accumulates in the cytoplasm to be detected by PKR is currently under investigation.

Our data indicated that PKR interacts with a species of IL-24, which has been at least partially deglycosylated. Furthermore, ubiquitination of IL-24 at K123 is not required as the isoform missing this site, IL-24 ΔEx5, can also be immunoprecipitated by PKR. Further studies are required to establish whether other ubiquitinated lysines or any posttranslational modifications facilitate this interaction. PKR-interacting proteins such as TRBP and ADAR1 have double-stranded RNA binding domains (dsRBDs) that interact with PKR's own dsRBDs (66, 67). IL-24 does not have a canonical dsRBD αββα fold structure, so it is unlikely that it interacts with PKR in this way (68). In contrast, PACT binds to a

specific motif in PKR's kinase domain to disrupt PKR autoinhibitory conformation (69); it is possible that IL-24 may activate PKR in a similar way. Further investigation is required to determine the specific regions critical for IL-24–PKR interaction. An alternative hypothesis is that PKR and IL-24 may not interact directly, instead they may be two integral parts of a larger complex. PKR is well-known to be activated in stress granules, and it is conceivable that cytoplasmic IL-24 could provide the basis for stress granule formation and thereby lead to activation of PKR. Unbiased screens are one way to reveal other key players in the inflammatory response to proteasome dysfunction.

It is intriguing that PRAAS patient fibroblasts exhibited increased expression of shorter IL-24 mRNA species, particularly after cell stress in the form of serum starvation. This implies that there may be active mechanisms that regulate IL-24 transcription and splicing, which are altered in response to proteasome dysfunction. One such mechanism could be by the splicing factor, arginine/ serine-rich (SRSF) family member SRSF6 (previously known as SRp55), a splice factor capable of regulating IL-24 mRNA (36), and this may be linked to cellular stress (38). A positive correlation between proteasome inhibitor–induced stress, SRSF phosphorylation, and alternative exon selection has been reported (70). Primary cells from patients affected by PRAAS are hyperresponsive to IFN stimulation, and environmental factors such as infection or stress can trigger inflammatory flares of disease. Therefore, it will be interesting to determine whether this is associated with factors that regulate IL-24 transcription and/or isoform expression with an increased propensity for the cytokine to be sent for ERAD, whereupon it activates PKR.

In summary, here we presented a pathway by which proteasome dysfunction triggers the innate immune sensor PKR, mediated by cytosolic accumulation of a cytokine, IL-24. These findings have significant implications not only for PRAAS but also for other diseases associated with proteotoxic stress and inflammation such as neurodegenerative disorders, where activation of PKR has also been observed.

MATERIALS AND METHODS

Study design

The objective of this study was to identify PRRs and ligands driving inflammation in the autoinflammatory disease PRAAS. We developed a cellular model for PRAAS using CRISPR-Cas9 gene editing to delete PRAAS-associated genes in primary cells and cell lines and confirmed the inflammatory phenotype using Western blotting, enzyme-linked immunosorbent assay (ELISA), flow cytometry, and qPCR. We also confirmed that chemical inhibition of the proteasome drove a similar inflammatory response. Using these two independent model systems, we screened a range of cell types deficient in key PRRs and later known ligands to identify and confirm a mechanism of inflammation in PRAAS. Further investigation of PRR and ligand interaction was performed using super-resolution imaging, immunoprecipitation, and cellular fractionation. Last, we applied the same techniques to analyze this pathway in PRAAS patient cells.

Cell culture, reagents, and inhibitors

Human THP-1 cells were obtained from the American Type Culture Collection (catalog no. TIB-202) and cultured in RPMI 1640 [prepared in-house, RPMI 1640 powder (Life Technologies), 23.8 mM sodium bicarbonate ($NaHCO_3$) (Merck), 1 mM sodium pyruvate ($C_3H_3NaO_3$) (Sigma-Aldrich), penicillin (100 U/ml; Sigma-Aldrich), and streptomycin (100 μg/ml; Sigma-Aldrich)] supplemented with 10% fetal calf serum (FCS) (Sigma-Aldrich). Human U2OS cells [a gift from I. Lucet, Walter and Eliza Hall Institute of Medical Research (WEHI)] and human embryonic kidney (HEK) 293T cells were maintained in Dulbecco's modified Eagle's medium (DMEM) (Gibco), 40 mM $NaHCO_3$, penicillin (100 U/ml; Sigma-Aldrich), and streptomycin (100 μg/ml; Sigma-Aldrich) supplemented with 10% FCS. Immortalized MEFs lacking MAVS (71), PKR (72), STING (73), or wild-type (WT) controls (72, 73) were described previously. These MEF lines were maintained in DMEM medium supplemented with 10% FCS, penicillin (100 U/ml), and streptomycin (100 μg/ml). UNC93B1$^{-/-}$ or C57BL/6 bone marrow cells from 9-week-old female mice (a gift from A. Marshak-Rothstein, University of Massachusetts Medical School) were obtained by flushing femurs and tibias with 10% FCS DMEM using a 23-gauge needle. Red blood cells were lysed using ammonium chloride, and cells were cultured in macrophage colony-stimulating factor (M-CSF) (20 ng/ml; Peprotech) supplemented with 10% FCS, l-glutamine, penicillin, streptomycin, and β-mercaptoethanol in DMEM. Medium was replaced at day 4, and macrophages were harvested at day 7 by collection of the adherent cells. THP-1 cells were cultured at 37°C in a humidified atmosphere with 5% CO_2; all other cell lines were cultured in a humidified atmosphere with 10% CO_2. For all THP-1 experiments, cells were cultured at 0.5 to 1 × 10^6 cells/ml in 24-well plates (Corning), unless otherwise stated. Bone marrow–derived macrophages and MEFs were seeded at 0.5 × 10^6 cells per well in six-well plates (Corning) and allowed to adhere overnight before stimulation. mtDNA-depleted cells (THP-1 ρ^0) were generated as previously described (24). Briefly, THP-1 cells were cultured in 10% FCS in RPMI 1640 containing ethidium bromide (50 ng/ml), sodium pyruvate (100 μg/ml), and uridine (50 μg/ml) for 3 weeks and then rested for an additional 2 weeks in the presence of uridine. Depletion was assessed using real-time qPCR for mtDNA and nuclear genes. To estimate mtDNA content in ρ^0 cells, qPCR results were converted into percentage based on expression of corresponding mtDNA gene in control cells (fig. S2G). As extra confirmation, we quantified the change in the mtDNA binding protein, TFAM, by immunoblot (fig. S2H). Cells were treated for specified time periods with the following: PR619 (5 μM; Sigma-Aldrich), delanzomib (200 nM; Sellekchem), oprozomib (500 nM; Sellekchem), C16 (0.5 μM; Sigma-Aldrich), kifunesine (50 nM; Sigma-Aldrich), DMJM (100 nM; Sigma-Aldrich), SW (1000 nM; Sigma-Aldrich), 4μ8c (100 μM; Merck-Millipore), or guanabenz (50 μM, Merck-Millipore) unless otherwise stated. cGAMP (10 μg/ml; InvivoGen) and poly(dA:dT) (1 μg/ml; InvivoGen) were transfected into cells using Lipofectamine 2000 (Life Technologies) diluted in Opti-MEM as per the manufacturer's instructions. cGAMP, poly(dA:dT), kifunesine, and DMJM were all reconstituted in dH_2O, SW was reconstituted in methanol, and all other reagents were solubilized in dimethyl sulfoxide (DMSO) (Sigma-Aldrich). Equivalent amounts of dH_2O, methanol, and DMSO were used for vehicle controls as appropriate.

Patient samples

The fibroblast cell lines, iPSC PBMCs, and expanded T cell samples used in the paper were generated from skin biopsies or blood draws from patients and HCs at the National Institutes of Health (NIH), Texas Children's Hospital-Baylor College of Medicine, or WEHI after obtaining consent. NIH Institutional Review Board–approved natural human history study (www.clinicaltrials.gov/ct2/show/NCT02974595) NIH #17-I-0016 "Studies of the natural history, pathogenesis, and outcome of autoinflammatory diseases", Baylor College of Medicine ethics number: H-21453, WEHI Human ethics number: HREC ID 18/07, University of Greifswald ethics number BB 209/18. The use of the buffy coat obtained from healthy volunteers to prepare PBMCs was approved by the ethics board of the Universitätsmedizin Greifswald under the condition that the samples were fully anonymized and could not be traced back to the individual patient (ethics number BB 014/14). All patient mutations used in this study have been previously published and are listed in table S2. PBMCs were isolated from whole blood using Ficoll (GE Healthcare), frozen in FCS with 10% DMSO, and stored in liquid nitrogen (long term) or −80°C (short term) until use. PBMCs were treated with 0.5 μM C16 (1×10^6 cells per condition) or vehicle Ctrl (DMSO, Sigma-Aldrich) and cultured in 10% FCS RPMI 1640 at 37°C in a humidified atmosphere with 5% CO_2 for 8 to 14 hours before lysis and downstream analysis. Fibroblasts were cultured in 10% DMEM at 37°C in a humidified atmosphere with 5% CO_2.

CRISPR-Cas9 gene editing

CRISPR-Cas9 gene editing was used to generate *PSMB8*$^{-/-}$ (iβ5$^{-/-}$), *PSMB9*$^{-/-}$ (iβ1$^{-/-}$), *UNC93B1*$^{-/-}$, *MAVS*$^{-/-}$, *TMEM173*$^{-/-}$ (STING$^{-/-}$), *EIF2AK2*$^{-/-}$ (PKR$^{-/-}$), *PSMB8*$^{-/-}$*EIF2AK2*$^{-/-}$ (iβ5$^{-/-}$PKR$^{-/-}$), *EIF2AK1*$^{-/-}$ (HRI$^{-/-}$), *EIF2AK3*$^{-/-}$ (PERK$^{-/-}$), *EIF2AK4*$^{-/-}$ (GCN2$^{-/-}$), *TARBP2*$^{-/-}$, *PRKRA*$^{-/-}$ (PACT$^{-/-}$), *IL24*$^{-/-}$, *PSMB8*$^{-/-}$*IL24*$^{-/-}$ (iβ5$^{-/-}$IL-24$^{-/-}$), *PSMB9*$^{-/-}$*IL24*$^{-/-}$ (iβ1$^{-/-}$IL-24$^{-/-}$), and *IL20RB*$^{-/-}$ THP-1 cell lines as described (74). Lipofectamine 2000 (Life Technologies) was used to transfect HEK293T cells according to the manufacturer's instructions; FUCas9mCherry construct and the doxycycline-inducible FgH1tUTG construct are available from Addgene (plasmid numbers 70183 and 70182), and targeting guide sequences that were generated using CHOPCHOP software (75) are listed in table S1. To induce deletion, THP-1 cell lines were treated with doxycycline (1 μg/ml; Sigma-Aldrich) for 48 to 72 hours. Cells were then washed and allowed to rest in standard culture media overnight before running of experiments. Deletion was confirmed at the protein level by Western blot or for mRNA by qPCR. Cas9-expressing THP-1 cells (THP-1s) generated in parallel were used as reference parental cell line.

Cytokine measurements

To measure protein levels of CXCL10 and IFN-β, iβ5$^{-/-}$, iβ1$^{-/-}$, and THP1 cell lines were seeded at 3×10^5 cells per well in 96-well plate after 72 hours of doxycycline treatment and 24 hours of rest. Twenty-four hours later, culture supernatants were collected, and CXCL10 and IFN-β concentration were measured by ELISA using the Human CXCL10/IP-10 Quantikine ELISA Kit, R&D Systems, and the VeriKine-HS Human IFN-β Serum ELISA Kit.

Immunoblotting

Cells and tissues were lysed in 1× KALB buffer [1% Triton X-100, 50 mM tris-HCl (pH 7.4), 150 mM NaCl, 1 mM EDTA, 10 mM NaPPi, 5 mM NaF, and 1 mM Na_3VO_4] or 1× radioimmunoprecipitation assay (RIPA) buffer [1% Triton X-100, 20 mM tris-HCl (pH 7.4), 150 mM NaCl, 1 mM EDTA, 0.5% sodium deoxycholate, 3.5 mM SDS, 10% glycerol, 10 mM NaPPi, 5 mM NaF, and 1 mM Na_3VO_4] supplemented with 1 mM phenylmethylsulfonyl fluoride and cOmplete protease inhibitors (Roche Biochemicals) for 20 min at 4°C. Protein content of in vivo samples was normalized after quantitation by bicinchoninic acid (BCA) assay (Thermo Fisher Scientific). Samples were processed through Pierce centrifuge columns (Thermo Fisher Scientific) to remove DNA. After addition of reducing SDS– polyacrylamide gel electrophoresis (SDS-PAGE) sample loading buffer [1.25% SDS, 12.5% glycerol, 62.5 mM tris-HCl (pH 6.8), 0.005% bromophenol blue, and 50 mM dithiothreitol] and denaturation at 95°C for 5 to 10 min, samples were separated on Novex 4 to 12% precast SDS-PAGE gels (Thermo Fisher Scientific) with MES running buffer (Thermo Fisher Scientific) and subsequently transferred onto polyvinylidene difluoride membrane (Millipore). Membranes were blocked in 5% skim milk in tris-buffered saline (TBS) containing 0.1% Tween 20 (Sigma-Aldrich) (TBST) before overnight incubation with specific primary antibodies in 5% bovine serum albumin (BSA) (Sigma-Aldrich) or 5% skim milk in TBST at 4°C: anti-ubiquitin (Santa Cruz Biotechnology, clone P4D1, sc-8017), anti–phosphor-p65 Ser^{536} [Cell Signaling Technology (CST), clone 93H1, 3033], anti-iβ5 (Abcam, ab3329), anti-iβ1 (Thermo Fisher Scientific, PA11960), anti–phosphor-PKR Thr^{446} (Abcam, clone E120, ab32036), anti–phosphor-eIF2α Ser^{51} (CST, clone D9G8, 3398), anti-TFAM (CST, clone D5C8, 8076), anti–phosphor-STAT1 Tyr^{701} (CST, clone 58D6, 9167), anti–IL-24 (R&D Systems, AF1965, or Abcam, ab115207), anti-PACT (Santa Cruz Biotechnology, clone D-4, sc-377103), anti-TRBP (Santa Cruz Biotechnology, clone D-5, sc-514124), or anti–actin–horseradish peroxidase (HRP) (1:10,000; Santa Cruz Biotechnology, clone C4, sc-47778). All listed primary antibodies were used at 1:1000 unless otherwise stated. Membranes were washed three times with TBST and incubated with appropriate HRP-conjugated secondary antibodies and washed again three times. Last, membranes were developed (Chemiluminescent HRP Substrate, Millipore) and imaged using the ChemiDoc Touch Imaging System (Bio-Rad) or film (GE Healthcare or Thermo Fisher Scientific).

Flow cytometry

Cell lines were analyzed for levels of phosphor-STAT1, total STAT1, and IFN-α as previously described (3, 76). Briefly, cells were cultured at 1×10^6 cells/ml for 6 to 8 hours with brefeldin A (1 μg/ml; Sigma-Aldrich), washed 1× with PBS (Thermo Fisher Scientific), and resuspended in residual volume. Samples were fixed by adding 1 ml of BD Phosflow Lyse/Fix Buffer (BD Biosciences) per tube and incubated at room temperature for 15 to 20 min. Samples were then washed 1× with PBS, resuspended in residual volume, and permeabilized by adding prechilled Perm Buffer II (BD Biosciences) dropwise while vortexing and incubating on ice for 40 min. Samples were washed 1× with PBS and then stained with the following primary antibodies: anti–IFN-α (PBL Interferon Source, clone MMHA-11, 21112-3), anti–phosphor-STAT1 Tyr^{701} (CST, clone 58D6, 9167), or anti-STAT1 (CST, clone D1K9Y, 14994) overnight at 4°C in the dark. Samples were then

washed 2× with PBS and incubated with a goat anti-rabbit AF647 secondary antibody (Life Technologies, A21245 and A21447) and washed again 3×. Staining for IL-24 (1:200; R&D Systems, AF1965, donkey anti-goat AF647 secondary antibody (Abcam, ab150131) was performed using the same method; however, culture with brefeldin A was not performed. To confirm IL-24–Halo expression in U2OS cells after antibiotic selection, 2×10^5 U2OS parental and IL-24–Halo–expressing cells were stained with Janelia Fluor 646 HaloTag (1:10,000; Promega, GA1120) in 2% FCS PBS for 15 min on ice. Samples were then washed 2× before downstream analysis. To determine cell viability under kifunesine, DMJM, or SW treatment, THP-1 cells were stained with propidium iodide (1 μg/ml; Thermo Fisher Scientific) in 2% FCS PBS for 15 min on ice and then washed 2×. All samples were resuspended in PBS and analyzed using BD LSR Fortessa X-20 (Becton Dickinson) and FlowJo 10 software (FlowJo).

Real-time qPCR for cell lines

For experiments using THP-1 or MEF cell lines or bone marrow– derived macrophages, total RNA was isolated using the ISOLATE II RNA Mini Kit (Bioline) as per the manufacturer's instructions. Deoxyribonuclease (DNase)–treated total RNA (0.5 to 1 μg) was reverse-transcribed using oligo(dT) nucleotides (Promega) to generate complementary DNA (cDNA). qPCR was performed using SYBR Green/ROX qPCR Master Mix (Thermo Fisher Scientific) on a ViiA 7 Real-Time PCR system (Thermo Fisher Scientific). Primers for cytokines, mDNA, and housekeeping genes were used as described previously (73, 77). Each sample was run in duplicate, and samples were normalized using the housekeeping gene *HRPT*. Results were analyzed using the $\Delta\Delta C_t$ method and represented as fold change of vehicle-control–treated parental (THP-1) or WT (MEF and mouse primary cells) sample from the same experiment.

For PBMC samples, cell lysis and total RNA extraction were performed with TRIzol reagent (Invitrogen) as per the manufacturers' instructions. cDNA was generated from 0.3 to 1 μg of DNase-treated total RNA using the Invitrogen SuperScript III First-Strand Synthesis System for reverse transcription PCR (RT-PCR) (Invitrogen). qPCR experiments were performed using TaqMan probes (Life Technologies), sequences were previously published (78). Each sample was run in triplicate, and samples were normalized using the housekeeping genes 18*S* or *HPRT*. Results were analyzed using the $\Delta\Delta C_t$ method and represented as fold change of vehicle-treated HC sample from the same experiment.

Treatment of mice with proteasome inhibitors

PKR-deficient mice ($PKR^{-/-}$ mice) on a C57BL/6 background (79) were studied at WEHI compared with littermate control mice. Aged matched male and female mice 8 to 12 weeks old were used. Mice were injected intraperitoneally with bortezomib (1 mg/kg; SelleckChem, S1013), and after 18 hours, mice were humanely euthanized, and cardiac puncture and splenectomy were performed. Whole-blood cell lysis and total RNA extraction were performed using TRIzol reagent (Invitrogen) as per the manufacturer's instructions. Spleens were passed through a 70 μM cell strainer to generate a single-cell suspension, and red blood cell lysis was performed using red blood cell lysis buffer and halted with excess 2% FCS PBS. Spleen samples were then lysed for RNA extraction, and RNA

was isolated using the ISOLATE II RNA Mini Kit (Bioline) as per the manufacturer's instructions. A total of 0.3 μg (blood) or 1 μg (spleen) of DNase-treated total RNA was reverse-transcribed using oligo(dT) nucleotides (Promega) to generate cDNA. *Il24*$^{-/-}$ mice on the 129 background (*B6N(Cg)-Il24tm1.1(KOMP)Vlcg/2 J* (80) were originally purchased via KOMP/the Jackson Laboratory (Bar Harbor, ME) and backcrossed at the National Institute of Allergy and Infectious Diseases (NIAID) to Taconic C57BL/6 (used as control) for an additional 10 generations. Male mice 8 to 24 weeks old at onset of experiments were used, and experimental groups in individual experiments were age-matched. Mice were injected intraperitoneally with bortezomib (1 mg/kg; SelleckChem, S1013). After 7 hours, mice were humanely euthanized, and spleens were harvested and homogenized in icecold RIPA buffer supplemented with protease and phosphatase inhibitors for protein extraction. Samples were normalized for protein concentration using the Pierce BCA Protein Assay Kit (Thermo Fisher Scientific).

At WEHI, animal procedures were approved by the WEHI Animal Ethics Committee (Ethics application: 2020.017). At NIAID, animals were bred and maintained in an Association for Assessment and Accreditation of Laboratory Animal Care International–accredited animal biosafety level 2 facility, and experiments were performed in compliance with an animal study proposal approved by the NIAID Animal Care and Use Committee.

Exogenous IL-24 expression

To generate stable IL-24 and IL-24 ΔEx5–expressing cell lines, sequences were obtained from UniProt and double-stranded DNA gBlocks were ordered from IDT Technologies with the addition of an Age I 5′ cloning site, C-terminal tag of either hemagglutinin (HA) (for THP-1 experiments) or Halo (for U2OS experiments), and a Bam HI 3′ cloning site (table S3). Cas9 was cut out from the lentiCas9-Blast lentiviral construct, and IL-24 gBlocks were cloned in [lentiCas9-Blast was from F. Zhang (Addgene, plasmid no. 52962) (81)]. Sanger sequencing was performed to confirm complete and correct insertion. HEK293T cells were transiently transfected with IL-24 lenti-Blast or IL-24 ΔEx5 lenti-Blast plasmids, pMDL (packaging), RSV-REV (packaging), and VSVg (envelope) using Lipofectamine 2000 diluted in Opti-MEM (Thermo Fisher Scientific) to generate lentiviral particles. The cell culture supernatant was collected 48 hours later and passed through a 0.45-μm filter before transduction. Target cells (3×10^6) were centrifuged with the lentivirus in the presence of polybrene (Sigma-Aldrich) at 839*g* for 3 hours at room temperature and cultured at 37°C overnight. Transduced cells were washed and subjected to antibiotic selection with blasticidin (2 μg/ml; Thermo Fisher Scientific) for 2 weeks to generate stable cell lines. For transient expression in HEK293T cells, 1 μg of each IL-24 plasmid was transfected using Lipofectamine 2000 diluted in Opti-MEM (Thermo Fisher Scientific) and left overnight. HEK293T cells were washed the next day and left for a further 24 hours before lysis and analysis by immunoblot.

Plasmid mutagenesis

The lenti-Blast construct IL-24 N86Q, N99Q, and N126Q were obtained via site-directed mutagenesis of the IL-24 lenti-Blast plasmid using the QuikChange Lightning Kit (Agilent

Technologies). Oligonucleotide primers are listed in table S4, and mutagenesis was confirmed via Sanger sequencing.

Immunoprecipitation

Patient fibroblasts, THP-1, iβ5$^{-/-}$, iβ5$^{-/-}$PKR$^{-/-}$ or iβ5$^{-/-}$IL-24$^{-/-}$, THP-1 + IL-24, iβ5$^{-/-}$ + IL-24, iβ5$^{-/-}$PKR$^{-/-}$ + IL-24, THP-1 + IL-24 ΔEx5, iβ5$^{-/-}$ + IL-24 ΔEx5, and iβ5$^{-/-}$PKR$^{-/-}$ + IL-24 ΔEx5 cells were cultured for 16 hours with PR619 (5 μM; Sigma-Aldrich). A minimum of 3×10^7 THP-1 cells or 1×10^7 fibroblasts per condition were used. Because of poor growth, fibroblasts from PRAAS#1 to 3 patients had to be pooled. Cells were lysed in 1 to 1.5 ml of KALB buffer at 4°C for 20 min and then processed through Pierce centrifuge columns (Thermo Fisher Scientific) to remove DNA. A total of 50 μl of each sample was kept for WCL and processed as per immunoblot samples. A total of 10 μg of PKR antibody agarose conjugate beads (Santa Cruz Biotechnology, clone B-10, sc-6282) was added per 1 ml of lysate and incubated at 4°C for 4 hours on a rotator. Samples were washed 3× with KALB buffer and resuspended in 30 μl of sample buffer. Samples were then boiled for 5 min and subjected to immunoblotting (as per the “Immunoblotting” section).

PNGase F treatment

A total of 5×10^6 iβ5$^{-/-}$ + IL-24 cells were lysed under denaturing conditions in 50 μl as per New England Biolabs Inc. PNGase F kit protocol. Glycoprotein was denatured by heating reaction at 100°C for 10 min, chilled on ice, and then centrifuged at a maximum speed for 10 s. A total of 10 μl of lysate was taken and made up to 20 μl by adding 2 μl of 10× GlycoBuffer 2, 2 μl of 10% NP-40, and 6 μl of H_2O. One microliter of PNGase F was added, and reaction and both samples were incubated at 37°C for 1 hour. Two separate control samples were also prepared, one taken before PNGase F treatment (CTRL) and one incubated at 37°C for 1 hour without enzyme (37°C CTRL). SDS loading buffer was added to samples for downstream analysis by immunoblot.

Immunofluorescence

For super-resolution and lattice light-sheet imaging, U2OS cells stably expressing IL-24–Halo tag were seeded at 1×10^4 cells per well in eight-well chamber slides (iBidi, 80826) and allowed to adhere overnight. Thirty minutes before imaging, cells were incubated with Janelia Fluor 646 HaloTag (1:10,000; Promega, GA1120), ER-Tracker Red, and 4′,6-diamidino-2-phenylindole (DAPI) [Thermo Fisher Scientific, E34250 (1:1000) and D1306 (1:10,000)]. Each iBidi slide was mounted in the imaging chamber before drug treatment. Cells were treated with delanzomib, kifunesine, vehicle control (Ctrl), or stated combination thereof. Three-color super-resolution imaging was performed on the Zeiss LSM 880 NLO with fast Airyscan Confocal microscope, with Airyscan detection. For quantification, surfaces were created for IL-24–Halo and ER Tracker and spatial calculation of the proportion of IL-24-Halo dissociated with ER-Tracker was then performed using Imaris v8 to 9 software (Bitplane). Display images were processed into maximum intensity projections using Fiji software. The lattice light-sheet microscope used in these experiments is housed in the Centre for Dynamic Imaging at the WEHI. Time-lapse live-cell data were acquired using a Lattice Light Sheet 7 (Zeiss, Pre-serial). Light sheets (561 nm and 633 nm) 30 μm in length with a thickness of 1 μm were created at the sample plane via a 13.3

×0.44 numerical aperture (NA) objective. Fluorescence emission was collected via a 44.83 ×1 NA detection objective. Aberration correction was set to a value of 182 to minimize aberrations as determined by imaging the Point Spread Function using 170-μm fluorescent microspheres. Resolution was determined to be 454 nm (lateral) and 782 nm (axial). Data were collected with a frame time of 20 ms and a *z* step of 0.2 μm with 1251 frames per 250 μm by 250 μm volume every 10 min for the duration of the acquisition. Light was collected via a multiband stop, LBF 405/488/561/633, filter. Data were subsequently deskewed and then deconvolved using a constrained iterative algorithm and 20 iterations. Three-dimensional data were visualized and rendered using Imaris (Bitplane). For fixed imaging, glass coverslips (18 mm by 18 mm, thickness 1½, Zeiss) were coated overnight, 4°C, with RetroNectin (80 μg/ml; Takada, T202). Slides were washed 1× with PBS and blocked with 2% BSA in PBS for 30 min at room temperature. Slides were washed with PBS and then placed into six-well plates (one slide per well). THP-1 cells stably expressing HA-tagged IL-24 or ΔEx5 IL-24 were seeded at 3×10^5 cells per well and cultured for 72 hours with phorbol 12-myristate 13-acetate (PMA) (100 ng/ml) in 10% FCS in DMEM (culture medium) to drive differentiation and adherence to slides. After 72 hours, medium was replaced with fresh culture medium, and cells were allowed to rest overnight. Cells were then treated with delanzomib or vehicle control (Ctrl) for 14 hours. Cells were then fixed in 4% paraformaldehyde (Electron Microscopy Sciences) and blocked for 1 hour in 3% normal goat serum and 0.1% Triton X-100 in PBS [immunofluorescence (IF) staining buffer]. Slides were then incubated overnight at 4°C with anti–HA-DyLight 488 (1:500; Invitrogen, clone 2–2.2.14, 26183-D488) in IF staining buffer. Slides were then washed 3× with IF wash buffer (0.1% Triton-X100 in PBS) and mounted onto microscopy slides using Fluoromount-G with DAPI (Thermo Fisher Scientific). Two-color imaging was performed on the SP8 LIGHTNING Confocal Microscope (Leica Microsystems). All display images were processed into maximum intensity projections using Fiji software.

Analysis of IL-24 splice variants

Patient and HC fibroblasts were seeded into 10-cm^2 dishes at 1.5×10^5 cells per dish and allowed to grow to ~70% confluency over 72 hours. Cells were then washed 3× with PBS (Thermo Fisher Scientific). Medium was replaced with either DMEM only (serumstarved) or 10% FCS DMEM, and cells were harvested 18 hours later. Total RNA was isolated using TRIzol reagent (Invitrogen), and 1 μg of DNase-treated total RNA was reverse-transcribed using oligo(dT) nucleotides (Promega) to generate a cDNA template. To amplify the entire open reading frame of any *IL24*, splice isoform containing the first and last exons of *IL24* primers complementary to exons 1 and 7 were used, and β-tubulin mRNA was amplified as a control (39). RT-PCR was performed as previously done (39), and PCR products were separated on 1% agarose gels containing of Gel Red (0.5 μg/ml; Sigma-Aldrich) at 1 V/cm in tris-borate EDTA (TBE) buffer (Thermo Fisher Scientific).

Nanostring and ISG score

Healthy control or patient PBMCs were thawed and immediately treated for 8 to 14 hours with 0.5 μM C16 (1×10^6 cells per condition) or vehicle Ctrl (DMSO, Sigma-Aldrich). Total RNA was extracted using TRIzol reagent (Life Technologies, Carlsbad, CA), and 200 ng of RNA per sample was used. The level of ISG induction (ISG score) was

assessed using a customized NanoString assay (78). Gene expression of 28 ISGs and four housekeeping genes was measured according to the manufacturer's recommendations (NanoString Technologies). A total of 200 ng of RNA per sample was used. Data were processed with nSolver software (NanoString Technologies), which included assessment of quality of the runs. Data were combined, normalized, and analyzed in Excel (Microsoft Corporation).

Subcellular fractionation

Subcellular fractionation was performed as per Yu *et al.* (82). Briefly, 5×10^6 HC or PRAAS patient fibroblasts were collected, 10% of samples was lysed in 50 μl of KALB for WCL, whereas the remaining 90% of each sample was lysed in 100 μl of 0.0045% digitonin/MELB buffer [20 mM Hepes-KOH (pH 7.5), 250 mM sucrose, 1 mM EDTA, 50 mM KCl, and 2.5 mM $MgCl_2$] at 4°C for 10 min. Cell lysates were centrifuged twice at 13,000*g* for 5 min at 4°C to separate the cytosolic fraction from a pellet that contains the heavy membrane fraction. The cytosolic portion was collected, the heavy membrane pellet was discarded, and the loading buffer was then added to all samples for downstream analysis by immunoblot.

iPSC culture and differentiation

The following established human iPSC lines were used in this study; a control line (NCRM-1, denoted HC in this manuscript) from the National Institute of Neurological Disorders and Stroke (83) and one PRAAS (#3) patient from the laboratory of R.G.M. All iPSCs were maintained at 37°C with 5% CO_2 on Matrigel-coated (Corning, 354277) six-well plates in mTeSR1 (STEMCELL Technologies, 85850) containing 1× Primocin (InvivoGen, ant-pm-1) and passaged 1:6 using ReLeSR (STEMCELL Technologies, 05872) with Rho-associated, coiled-coil containing protein kinase inhibitor Y-27632 (STEMCELL Technologies, 72304) for the first 24 hours. The medium was replaced daily. Cells were cyropreserved in mTeSR1/10% DMSO. A three-stage differentiation protocol was used to generate iPSC-derived macrophages. Hematopoietic progenitor cells were generated using the STEMdiff Hematopoietic Kit (STEMCELL Technologies, 05310) on Matrigel-coated plates as per the manufacturer's instructions. After 12 days of culture, nonadherent hematopoietic cells were collected and replated on tissue-coated six-well plates in expansion medium [Iscove's modified Dulbecco's medium (IMDM), 20% FCS, 1% penicillin-streptomycin, 5% protein-free hybridoma media II (Life Technologies), 0.1 mM 2-mercaptoethanol (Sigma-Aldrich), stem cell factor (SCF) (100 ng/ml; Peprotech, 300-07), Flt3-L (100 ng/ml; Peprotech, 300-19), IL-6 (100 ng/ml; Peprotech, 200-06), thrombopoietin (TPO) (10 ng/ml; Peprotech, 300-18), and IL-3 (10 ng/ml; Peprotech, AF-200-03)]. Hematopoietic cells were expanded for 2 to 3 days, and then nonadherent cells were collected and replated in fresh tissue culture plates in macrophage medium [IMDM, 10% FCS, 1% penicillin-streptomycin, 0.1 mM 2-ME, and human M-CSF (100 ng/ml; Peprotech, 300–25)], and cells were differentiated for 14 days, with media changed every 3 days.

Data representation and statistical analyses

Data are typically means ± SEM and unless otherwise stated, pooled from at least three independent experiments. For data generated from THP-1 and MEF cell lines, we used

ratio paired *t* tests to compare groups of paired values generated from multiple independent experiments. With the exception of Fig. 3H, where we compared independent measurements over time, here, a two-way analysis of variance (ANOVA) was used with Bonferrioni post tests to assess significance for individual time points. For in vivo experiments, each data point represents an individual mouse. We assumed parametric distribution of the data and assessed the difference between control and treatment groups using *t* tests. For experiments performed on ex vivo patient samples (Fig. 4B) where due to the nature of the samples, the data are nonnormally distributed, we used Wilcoxon matched-pair signed-rank test. GraphPad Prism 7 was used to generate all charts and perform all statistical analyses. A *P* value of <0.05 was considered significant.

Supplementary Material

Refer to Web version on PubMed Central for supplementary material.

Acknowledgments:

We would like to acknowledge C. L. Sweeny, B. Marrero, J. E. Vince, S. Nicholson, and A. Marshak-Rothstein for supplying reagents and technical advice or assistance.

Funding:

S.L.M acknowledges funding from the National Health and Medical Research Council (NHMRC) grants (1144282, 1142354, and 1099262), The Sylvia and Charles Viertel Foundation, HHMI-Wellcome International Research Scholarship, and Glaxosmithkline. S.D. acknowledges funding from NHMRC grants (GNT1143412 and GNT2003756). E.K. acknowledges funding from the German Research Foundation (SFBTR 167; RTG 2719/ B4). V.J.-C. acknowledges funding from FONDECYT no. 11181222. This work was supported in part by the intramural research program of NIAID (to K.D.M.-B., P.J.B, R.G.M., A.A.D.J., and A.M.). This research was funded in part by the Wellcome Trust (208694/Z/17/Z). For the purpose of open access, the author has applied a CC BY public copyright license to any author accepted manuscript version arising from this submission.

Data and materials availability:

All data needed to evaluate the conclusions in the paper are present in the paper or the Supplementary Materials.

REFERENCES AND NOTES

1. Manthiram K, Zhou Q, Aksentijevich I, Kastner DL, The monogenic autoinflammatory diseases define new pathways in human innate immunity and inflammation. Nat. Immunol 18, 832–842 (2017). [PubMed: 28722725]
2. Arima K, Kinoshita A, Mishima H, Kanazawa N, Kaneko T, Mizushima T, Ichinose K, Nakamura H, Tsujino A, Kawakami A, Matsunaka M, Kasagi S, Kawano S, Kumagai S, Ohmura K, Mimori T, Hirano M, Ueno S, Tanaka K, Tanaka M, Toyoshima I, Sugino H, Yamakawa A, Tanaka K, Niikawa N, Furukawa F, Murata S, Eguchi K, Ida H, Yoshiura KI, Proteasome assembly defect due to a proteasome subunit β type 8 (PSMB8) mutation causes the autoinflammatory disorder, Nakajo-Nishimura syndrome. Proc. Natl. Acad. Sci. U.S.A 108, 14914–14919 (2011). [PubMed: 21852578]
3. Brehm A, Liu Y, Sheikh A, Marrero B, Omoyinmi E, Zhou Q, Montealegre G, Biancotto A, Reinhardt A, Almeida de Jesus A, Pelletier M, Tsai WL, Remmers EF, Kardava L, Hill S, Kim H, Lachmann HJ, Megarbane A, Chae JJ, Brady J, Castillo RD, Brown D, Casano AV, Gao L, Chapelle D, Huang Y, Stone D, Chen Y, Sotzny F, Lee CCR, Kastner DL, Torrelo A, Zlotogorski A, Moir S, Gadina M, McCoy P, Wesley R, Rother K, Hildebrand PW, Brogan P, Krüger E, Aksentijevich I, Goldbach-Mansky R, Additive loss-of-function proteasome subunit mutations in

CANDLE/PRAAS patients promote type I IFN production. J. Clin. Invest 125, 4196–4211 (2015). [PubMed: 26524591]

4. de Jesus AA, Brehm A, Van Tries R, Pillet P, Parentelli A-S, Sanchez GAM, Deng Z, Paut IK, Goldbach-Mansky R, Krüger E, Novel proteasome assembly chaperone mutations in PSMG2/PAC2 cause the autoinflammatory interferonopathy CANDLE/ PRAAS4. J. Allergy Clin. Immunol 143, 1939–1943.e8 (2019). [PubMed: 30664889]
5. Kitamura A, Maekawa Y, Uehara H, Izumi K, Kawachi I, Nishizawa M, Toyoshima Y, Takahashi H, Standley DM, Tanaka K, Hamazaki J, Murata S, Obara K, Toyoshima I, Yasutomo K, A mutation in the immunoproteasome subunit PSMB8 causes autoinflammation and lipodystrophy in humans. J. Clin. Invest 121, 4150–4160 (2011). [PubMed: 21881205]
6. Liu Y, Ramot Y, Torrelo A, Paller AS, Si N, Babay S, Kim PW, Sheikh A, Lee CCR, Chen Y, Vera A, Zhang X, Goldbach-Mansky R, Zlotogorski A, Mutations in proteasome subunit β type 8 cause chronic atypical neutrophilic dermatosis with lipodystrophyand elevated temperature with evidence of genetic and phenotypic heterogeneity. Arthritis Rheum. 64, 895–907 (2012). [PubMed: 21953331]
7. Poli MC, Ebstein F, Nicholas SK, de Guzman MM, Forbes LR, Chinn IK, Mace EM, Vogel TP, Carisey AF, Benavides F, Coban-Akdemir ZH, Gibbs RA, Jhangiani SN, Muzny DM, Carvalho CMB, Schady DA, Jain M, Rosenfeld JA, Emrick L, Lewis RA, Lee B; Undiagnosed Diseases Network members, Zieba BA, Küry S, Krüger E, Lupski JR, Bostwick BL, Orange JS, Heterozygous truncating variants in POMP escape nonsense-mediated decay and cause a unique immune dysregulatory syndrome. Am. J. Hum. Genet 102, 1126–1142 (2018). [PubMed: 29805043]
8. Sarrabay G, Méchin D, Salhi A, Boursier G, Rittore C, Crow Y, Rice G, Tran T-A, Cezar R, Duffy D, Bondet V, Boudhane L, Broca C, Kant BP, Van Gijn M, Grandemange S, Richard E, Apparailly F, Touitou I, PSMB10, the last immunoproteasome gene missing for PRAAS. J. Allergy Clin. Immunol 145, 1015–1017.e6 (2020). [PubMed: 31783057]
9. Sanchez GAM, Reinhardt A, Ramsey S, Wittkowski H, Hashkes PJ, Berkun Y, Schalm S, Murias S, Dare JA, Brown D, Stone DL, Gao L, Klausmeier T, Foell D, de Jesus AA, Chapelle DC, Kim H, Dill S, Colbert RA, Failla L, Kost B, O'Brien M, Reynolds JC, Folio LR, Calvo KR, Paul SM, Weir N, Brofferio A, Soldatos A, Biancotto A, Cowen EW, Digiovanna JJ, Gadina M, Lipton AJ, Hadigan C, Holland SM, Fontana J, Alawad AS, Brown RJ, Rother KI, Heller T, Brooks KM, Kumar P, Brooks SR, Waldman M, Singh HK, Nickeleit V, Silk M, Prakash A, Janes JM, Ozen S, Wakim PG, Brogan PA, Macias WL, Goldbach-Mansky R, JAK1/2 inhibition with baricitinib in the treatment of autoinflammatory interferonopathies. J. Clin. Invest 128, 3041–3052 (2018). [PubMed: 29649002]
10. Griffin TA, Nandi D, Cruz M, Fehling HJ, Kaer LV, Monaco JJ, Colbert RA, Immunoproteasome assembly: cooperative incorporation of interferon-γ (IFN-γ)– inducible subunits. J. Exp. Med 187, 97–104 (1998). [PubMed: 9419215]
11. Seifert U, Bialy LP, Ebstein F, Bech-Otschir D, Voigt A, Schröter F, Prozorovski T, Lange N, Steffen J, Rieger M, Kuckelkorn U, Aktas O, Kloetzel PM, Krüger E, Immunoproteasomes preserve protein homeostasis upon interferon-induced oxidative stress. Cell 142, 613–624 (2010). [PubMed: 20723761]
12. Zhou HJ, Aujay MA, Bennett MK, Dajee M, Demo SD, Fang Y, Ho MN, Jiang J, Kirk CJ, Laidig GJ, Lewis ER, Lu Y, Muchamuel T, Parlati F, Ring E, Shenk KD, Shields J, Shwonek PJ, Stanton T, Sun CM, Sylvain C, Woo TM, Yang J, Design and synthesis of an orally bioavailable and selective peptide epoxyketone proteasome inhibitor (PR-047). J. Med. Chem 52, 3028–3038 (2009). [PubMed: 19348473]
13. Lind NA, Rael VE, Pestal K, Liu B, Barton GM, Regulation of the nucleic acid-sensing Toll-like receptors. Nat. Rev. Immunol, (2021).
14. Piva R, Ruggeri B, Williams M, Costa G, Tamagno I, Ferrero D, Giai V, Coscia M, Peola S, Massaia M, Pezzoni G, Allievi C, Pescalli N, Cassin M, di Giovine S, Nicoli P, de Feudis P, Strepponi I, Roato I, Ferracini R, Bussolati B, Camussi G, Jones-Bolin S, Hunter K, Zhao H, Neri A, Palumbo A, Berkers C, Ovaa H, Bernareggi A, Inghirami G, CEP-18770: A novel, orally active proteasome inhibitor with a tumor-selective pharmacologic profile competitive with bortezomib. Blood 111, 2765–2775 (2008). [PubMed: 18057228]

15. Ablasser A, Hur S, Regulation of cGAS- and RLR-mediated immunity to nucleic acids. Nat. Immunol 21, 17–29 (2020). [PubMed: 31819255]
16. Balachandran S, Roberts PC, Brown LE, Truong H, Pattnaik AK, Archer DR, Barber GN, Essential role for the dsRNA-dependent protein kinase PKR in innate immunity to viral infection. Immunity 13, 129–141 (2000). [PubMed: 10933401]
17. Oganesyan G, Saha SK, Guo B, He JQ, Shahangian A, Zarnegar B, Perry A, Cheng G, Critical role of TRAF3 in the Toll-like receptor-dependent and -independent antiviral response. Nature 439, 208–211 (2006). [PubMed: 16306936]
18. Gil J, García MA, Gomez-Puertas P, Guerra S, Rullas J, Nakano H, Alcamí J, Esteban M, TRAF family proteins link PKR with NF-κB activation. Mol. Cell. Biol 24, 4502–4512 (2004). [PubMed: 15121867]
19. Jammi NV, Whitby LR, Beal PA, Small molecule inhibitors of the RNA-dependent protein kinase. Biochem. Biophys. Res. Commun 308, 50–57 (2003). [PubMed: 12890478]
20. Sonenberg N, Hinnebusch AG, Regulation of translation initiation in eukaryotes: Mechanisms and biological targets. Cell 136, 731–745 (2009). [PubMed: 19239892]
21. Katze MG, Wambach M, Wong ML, Garfinkel M, Meurs E, Chong K, Williams BR, Hovanessian AG, Barber GN, Functional expression and RNA binding analysis of the interferon-induced, double-stranded RNA-activated, 68,000-Mr protein kinase in a cell-free system. Mol. Cell. Biol 11, 5497–5505 (1991). [PubMed: 1717830]
22. Meurs E, Chong K, Galabru J, Thomas NSB, Kerr IM, Williams BRG, Hovanessian AG, Molecular cloning and characterization of the human double-stranded RNA-activated protein kinase induced by interferon. Cell 62, 379–390 (1990). [PubMed: 1695551]
23. Kim Y, Park J, Kim S, Kim MA, Kang M-G, Kwak C, Kang M, Kim B, Rhee H-W, Kim VN, PKR senses nuclear and mitochondrial signals by interacting with endogenous double-stranded RNAs. Mol. Cell 71, 1051–1063.e6 (2018). [PubMed: 30174290]
24. Hashiguchi K, Zhang-Akiyama QM, Establishment of human cell lines lacking mitochondrial DNA. Methods Mol. Biol 554, 383–391 (2009). [PubMed: 19513686]
25. Patel RC, Sen GC, PACT, a protein activator of the interferon-induced protein kinase, PKR. EMBO J 17, 4379–4390 (1998). [PubMed: 9687506]
26. Park H, Davies MV, Langland JO, Chang HW, Nam YS, Tartaglia J, Paoletti E, Jacobs BL, Kaufman RJ, Venkatesan S, TAR RNA-binding protein is an inhibitor of the interferon-induced protein kinase PKR. Proc. Natl. Acad. Sci. U.S.A 91, 4713–4717 (1994). [PubMed: 7515177]
27. Pataer A, Vorburger SA, Chada S, Balachandran S, Barber GN, Roth JA, Hunt KK, Swisher SG, Melanoma differentiation-associated gene-7 protein physically associates with the double-stranded RNA–activated protein kinase PKR. Mol. Ther 11, 717–723 (2005). [PubMed: 15851010]
28. Logsdon NJ, Deshpande A, Harris BD, Rajashankar KR, Walter MR, Structural basis for receptor sharing and activation by interleukin-20 receptor-2 (IL-20R2) binding cytokines. Proc. Natl. Acad. Sci. U.S.A 109, 12704–12709 (2012). [PubMed: 22802649]
29. Uhlen M, Karlsson MJ, Zhong W, Tebani A, Pou C, Mikes J, Lakshmikanth T, Forsström B, Edfors F, Odeberg J, Mardinoglu A, Zhang C, von Feilitzen K, Mulder J, Sjöstedt E, Hober A, Oksvold P, Zwahlen M, Ponten F, Lindskog C, Sivertsson Å, Fagerberg L, Brodin P, A genome-wide transcriptomic analysis of protein-coding genes in human blood cells. Science 366, (2019).
30. Pataer A, Vorburger SA, Barber GN, Chada S, Mhashilkar AM, Zou-Yang H, Stewart AL, Balachandran S, Roth JA, Hunt KK, Swisher SG, Adenoviral transfer of the melanoma differentiation-associated gene 7 (mda7) induces apoptosis of lung cancer cells via up-regulation of the double-stranded RNA-dependent protein kinase (PKR). Cancer Res. 62, 2239–2243 (2002). [PubMed: 11956076]
31. Hirsch C, Blom D, Ploegh HL, A role for N-glycanase in the cytosolic turnover of glycoproteins. EMBO J. 22, 1036–1046 (2003). [PubMed: 12606569]
32. Fuson KL, Zheng M, Craxton M, Pataer A, Ramesh R, Chada S, Sutton RB, Structural mapping of post-translational modifications in human interleukin-24: Role of N-linked glycosylation and disulfide bonds in secretion and activity. J. Biol. Chem 284, 30526–30533 (2009). [PubMed: 19734147]

33. Caudell EG, Mumm JB, Poindexter N, Ekmekcioglu S, Mhashilkar AM, Yang XH, Retter MW, Hill P, Chada S, Grimm EA, The protein product of the tumor suppressor gene, melanoma differentiation-associated gene 7, exhibits immunostimulatory activity and is designated IL-24. J. Immunol 168, 6041–6046 (2002). [PubMed: 12055212]
34. Finger A, Knop M, Wolf DH, Analysis of two mutated vacuolar proteins reveals a degradation pathway in the endoplasmic reticulum or a related compartment of yeast. Eur. J. Biochem 218, 565–574 (1993). [PubMed: 8269947]
35. Wang F, Song W, Brancati G, Segatori L, Inhibition of endoplasmic reticulum-associated degradation rescues native folding in loss of function protein misfolding diseases. J. Biol. Chem 286, 43454–43464 (2011). [PubMed: 22006919]
36. Whitaker EL, Filippov V, Filippova M, Guerrero-Juarez CF, Duerksen-Hughes PJ, Splice variants of mda-7/IL-24 differentially affect survival and induce apoptosis in U2OS cells. Cytokine 56, 272–281 (2011). [PubMed: 21843952]
37. Filippov V, Schmidt EL, Filippova M, Duerksen-Hughes PJ, Splicing and splice factor SRp55 participate in the response to DNA damage by changing isoform ratios of target genes. Gene 420, 34–41 (2008). [PubMed: 18571879]
38. Sahoo A, Jung YM, Kwon HK, Yi HJ, Lee S, Chang S, Park ZY, Hwang KC, Im SH, A novel splicing variant of mouse interleukin (IL)-24 antagonizes IL-24-induced apoptosis. J. Biol. Chem 283, 28860–28872 (2008). [PubMed: 18708357]
39. Allen M, Pratscher B, Roka F, Krepler C, Wacheck V, Schöfer C, Pehamberger H, Müller M, Lucas T, Loss of novel mda-7 splice variant (mda-7s) expression is associated with metastatic melanoma. J. Invest. Dermatol 123, 583–588 (2004). [PubMed: 15304100]
40. Tian H, Li L, Zhang B, di J, Chen F, Li H, Liu J, Pei D, Zheng J, Critical role of lysine 123 in the ubiquitin-mediated degradation of MDA-7/IL-24. J. Interferon Cytokine Res 32, 575–582 (2012). [PubMed: 23078624]
41. Martinez C, Ebstein F, Nicholas SK, de Guzman M, Forbes LR, Delmonte OM, Bosticardo M, Castagnoli R, Krance R, Notarangelo LD, Krüger E, Orange JS, Poli MC, HSCT corrects primary immunodeficiency and immune dysregulation in patients with POMP-related autoinflammatory disease. Blood 138, 1896–1901 (2021). [PubMed: 34019630]
42. Tsaytler P, Harding HP, Ron D, Bertolotti A, Selective inhibition of a regulatory subunit of protein phosphatase 1 restores proteostasis. Science 332, 91–94 (2011). [PubMed: 21385720]
43. Chung H, Calis JJA, Wu X, Sun T, Yu Y, Sarbanes SL, Thi VLD, Shilvock AR, Hoffmann H-H, Rosenberg BR, Rice CM, Human ADAR1 prevents endogenous RNA from triggering translational shutdown. Cell 172, 811–824.e14 (2018). [PubMed: 29395325]
44. Gal-Ben-Ari S, Barrera I, Ehrlich M, Rosenblum K, PKR: A kinase to remember. Front Mol Neurosci 11, 480 (2019). [PubMed: 30686999]
45. Mouton-Liger F, Rebillat AS, Gourmaud S, Paquet C, Leguen A, Dumurgier J, Bernadelli P, Taupin V, Pradier L, Rooney T, Hugon J, PKR downregulation prevents neurodegeneration and β-amyloid production in a thiamine-deficient model. Cell Death Dis. 6, e1594 (2015). [PubMed: 25590804]
46. Couturier J, Paccalin M, Lafay-Chebassier C, Chalon S, Ingrand I, Pinguet J, Pontcharraud R, Guillard O, Fauconneau B, Page G, Pharmacological inhibition of PKR in APPswePS1dE9 mice transiently prevents inflammation at 12 months of age but increases Aβ42 levels in the late stages of the Alzheimer's disease. Curr. Alzheimer Res 9, 344–360 (2012). [PubMed: 22272616]
47. Carret-Rebillat AS, Pace C, Gourmaud S, Ravasi L, Montagne-Stora S, Longueville S, Tible M, Sudol E, Chang RCC, Paquet C, Mouton-Liger F, Hugon J, Neuroinflammation and Aβ accumulation linked to systemic inflammation are decreased by genetic PKR down-regulation. Sci. Rep 5, 8489 (2015). [PubMed: 25687824]
48. Gandolfi S, Laubach JP, Hideshima T, Chauhan D, Anderson KC, Richardson PG, The proteasome and proteasome inhibitors in multiple myeloma. Cancer Metastasis Rev. 36, 561–584 (2017). [PubMed: 29196868]
49. Parker BS, Rautela J, Hertzog PJ, Antitumour actions of interferons: Implications for cancer therapy. Nat. Rev. Cancer 16, 131–144 (2016). [PubMed: 26911188]

50. Alexander T, Sarfert R, Klotsche J, Kühl AA, Rubbert-Roth A, Lorenz HM, Rech J, Hoyer BF, Cheng Q, Waka A, Taddeo A, Wiesener M, Schett G, Burmester GR, Radbruch A, Hiepe F, Voll RE, The proteasome inhibitior bortezomib depletes plasma cells and ameliorates clinical manifestations of refractory systemic lupus erythematosus. Ann. Rheum. Dis 74, 1474–1478 (2015). [PubMed: 25710470]
51. Ishii T, Tanaka Y, Kawakami A, Saito K, Ichinose K, Fujii H, Shirota Y, Shirai T, Fujita Y, Watanabe R, Chiu SW, Yamaguchi T, Harigae H, Multicenter double-blind randomized controlled trial to evaluate the effectiveness and safety of bortezomib as a treatment for refractory systemic lupus erythematosus. Mod. Rheumatol 28, 986–992 (2018). [PubMed: 29363990]
52. McCarthy MK, Weinberg JB, The immunoproteasome and viral infection: A complex regulator of inflammation. Front. Microbiol 6, 21 (2015). [PubMed: 25688236]
53. Khu YL, Tan YJ, Lim SG, Hong W, Goh PY, Hepatitis C virus non-structural protein NS3 interacts with LMP7, a component of the immunoproteasome, and affects its proteasome activity. Biochem. J 384, 401–409 (2004). [PubMed: 15303969]
54. Khan S, Zimmermann A, Basler M, Groettrup M, Hengel H, A cytomegalovirus inhibitor of γ interferon signaling controls immunoproteasome induction. J. Virol 78, 1831–1842 (2004). [PubMed: 14747547]
55. Apcher GS, Heink S, Zantopf D, Kloetzel PM, Schmid HP, Mayer RJ, Krüger E, Human immunodeficiency virus-1 Tat protein interacts with distinct proteasomal α and β subunits. FEBS Lett. 553, 200–204 (2003). [PubMed: 14550573]
56. Vincent HA, Ziehr B, Moorman NJ, Mechanism of protein kinase R inhibition by human cytomegalovirus pTRS1. J. Virol 91, e01574–16 (2017). [PubMed: 27974558]
57. Pavio N, Taylor DR, Lai MM, Detection of a novel unglycosylated form of hepatitis C virus E2 envelope protein that is located in the cytosol and interacts with PKR. J. Virol 76, 1265–1272 (2002). [PubMed: 11773402]
58. Gale MJ Jr., Korth MJ, Tang NM, Tan SL, Hopkins DA, Dever TE, Polyak SJ, Gretch DR, Katze MG, Evidence that hepatitis C virus resistance to interferon is mediated through repression of the PKR protein kinase by the nonstructural 5A protein. Virology 230, 217–227 (1997). [PubMed: 9143277]
59. Brand SR, Kobayashi R, Mathews MB, The Tat protein of human immunodeficiency virus type 1 is a substrate and inhibitor of the interferon-induced, virally activated protein Kinase, PKR. J. Biol. Chem 272, 8388–8395 (1997). [PubMed: 9079663]
60. White MC, Schroeder RD, Zhu K, Xiong K, McConkey DJ, HRI-mediated translational repression reduces proteotoxicity and sensitivity to bortezomib in human pancreatic cancer cells. Oncogene 37, 4413–4427 (2018). [PubMed: 29720726]
61. Abdel-Nour M, Carneiro LAM, Downey J, Tsalikis J, Outlioua A, Prescott D, da Costa LS, Hovingh ES, Farahvash A, Gaudet RG, Molinaro R, van Dalen R, Lau CCY, Azimi FC, Escalante NK, Trotman-Grant A, Lee JE, Gray-Owen SD, Divangahi M, Chen JJ, Philpott DJ, Arnoult D, Girardin SE, The heme-regulated inhibitor is a cytosolic sensor of protein misfolding that controls innate immune signaling. Science 365, eaaw4144 (2019). [PubMed: 31273097]
62. Studencka-Turski M, Cetin G, Junker H, Ebstein F, Kruger E, Molecular insight into the IRE1α-mediated type I interferon response induced by proteasome impairment in myeloid cells of the brain. Front. Immunol 10, 2900 (2019). [PubMed: 31921161]
63. Suraweera A, Munch C, Hanssum A, Bertolotti A, Failure of amino acid homeostasis causes cell death following proteasome inhibition. Mol. Cell 48, 242–253 (2012). [PubMed: 22959274]
64. Kim DH, Park ES, Lee AR, Park S, Park YK, Ahn SH, Kang HS, Won JH, Ha YN, Jae BJ, Kim DS, Chung WC, Song MJ, Kim KH, Park SH, Kim SH, Kim KH, Intracellular interleukin-32γ mediates antiviral activity of cytokines against hepatitis B virus. Nat. Commun 9, 3284 (2018). [PubMed: 30115930]
65. Bartlett NW, Dumoutier L, Renauld JC, Kotenko SV, McVey CE, Lee HJ, Smith GL, A new member of the interleukin 10-related cytokine family encoded by a poxvirus. J. Gen. Virol 85, 1401–1412 (2004). [PubMed: 15166422]

66. Clerzius G, Gélinas JF, Daher A, Bonnet M, Meurs EF, Gatignol A, ADAR1 interacts with PKR during human immunodeficiency virus infection of lymphocytes and contributes to viral replication. J. Virol 83, 10119–10128 (2009). [PubMed: 19605474]

67. Daher A, Longuet M, Dorin D, Bois F, Segeral E, Bannwarth S, Battisti PL, Purcell DF, Benarous R, Vaquero C, Meurs EF, Gatignol A, Two dimerization domains in the trans-activation response RNA-binding protein (TRBP) individually reverse the protein kinase R inhibition of HIV-1 long terminal repeat expression. J. Biol. Chem 276, 33899–33905 (2001). [PubMed: 11438532]

68. Lubkowski J, Sonmez C, Smirnov SV, Anishkin A, Kotenko SV, Wlodawer A, Crystal structure of the labile complex of IL-24 with the extracellular domains of IL-22R1 and IL-20R2. J. Immunol 201, 2082–2093 (2018). [PubMed: 30111632]

69. Li S, Peters GA, Ding K, Zhang X, Qin J, Sen GC, Molecular basis for PKR activation by PACT or dsRNA. Proc. Natl. Acad. Sci. U.S.A 103, 10005–10010 (2006). [PubMed: 16785445]

70. Huang HH, Ferguson ID, Thornton AM, Bastola P, Lam C, Lin YHT, Choudhry P, Mariano MC, Marcoulis MD, Teo CF, Malato J, Phojanakong PJ, Martin III TG, Wolf JL, Wong SW, Shah N, Hann B, Brooks AN, Wiita AP, Proteasome inhibitor-induced modulation reveals the spliceosome as a specific therapeutic vulnerability in multiple myeloma. Nat. Commun 11, 1931 (2020). [PubMed: 32321912]

71. Nguyen TA, Smith BRC, Tate MD, Belz GT, Barrios MH, Elgass KD, Weisman AS, Baker PJ, Preston SP, Whitehead L, Garnham A, Lundie RJ, Smyth GK, Pellegrini M, O'Keeffe M, Wicks IP, Masters SL, Hunter CP, Pang KC, SIDT2 transports extracellular dsRNA into the cytoplasm for innate immune recognition. Immunity 47, 498–509.e6 (2017). [PubMed: 28916264]

72. Irving AT, Wang D, Vasilevski O, Latchoumanin O, Kozer N, Clayton AHA, Szczepny A, Morimoto H, Xu D, Williams BRG, Sadler AJ, Regulation of actin dynamics by protein kinase R control of gelsolin enforces basal innate immune defense. Immunity 36, 795–806 (2012). [PubMed: 22633459]

73. White MJ, McArthur K, Metcalf D, Lane RM, Cambier JC, Herold MJ, van Delft MF, Bedoui S, Lessene G, Ritchie ME, Huang DCS, Kile BT, Apoptotic caspases suppress mtDNA-induced STING-mediated type I IFN production. Cell 159, 1549–1562 (2014). [PubMed: 25525874]

74. Baker PJ, Masters SL, Generation of genetic knockouts in myeloid cell lines using a lentiviral CRISPR/Cas9 system. Methods Mol. Biol 1714, 41–55 (2018). [PubMed: 29177854]

75. Labun K, Montague TG, Krause M, Torres Cleuren YN, Tjeldnes H, Valen E, CHOPCHOP v3: Expanding the CRISPR web toolbox beyond genome editing. Nucleic Acids Res. 47, W171–W174 (2019). [PubMed: 31106371]

76. Fleisher TA, Dorman SE, Anderson JA, Vail M, Brown MR, Holland SM, Detection of intracellular phosphorylated STAT-1 by flow cytometry. Clin. Immunol 90, 425–430 (1999). [PubMed: 10075873]

77. Saldanha RG, Balka KR, Davidson S, Wainstein BK, Wong M, Macintosh R, Loo CKC, Weber MA, Kamath V; CIRCA; AADRY, Moghaddas F, de Nardo D, Gray PE, Masters SL, A mutation outside the dimerization domain causing atypical STING-associated vasculopathy with onset in infancy. Front. Immunol 9, 1535 (2018). [PubMed: 30038614]

78. Kim H, de Jesus AA, Brooks SR, Liu Y, Huang Y, VanTries R, Montealegre Sanchez GA, Rotman Y, Gadina M, Goldbach-Mansky R, Development of a validated interferon score using nanostring technology. J. Interferon Cytokine Res 38, 171–185 (2018). [PubMed: 29638206]

79. Yang YL, Reis LF, Pavlovic J, Aguzzi A, Schäfer R, Kumar A, Williams BR, Aguet M, Weissmann C, Deficient signaling in mice devoid of double-stranded RNA-dependent protein kinase. EMBO J. 14, 6095–6106 (1995). [PubMed: 8557029]

80. Dickinson ME, Flenniken AM, Ji X, Teboul L, Wong MD, White JK, Meehan TF, Weninger WJ, Westerberg H, Adissu H, Baker CN, Bower L, Brown JM, Caddle LB, Chiani F, Clary D, Cleak J, Daly MJ, Denegre JM, Doe B, Dolan ME, Edie SM, Fuchs H, Gailus-Durner V, Galli A, Gambadoro A, Gallegos J, Guo S, Horner NR, Hsu CW, Johnson SJ, Kalaga S, Keith LC, Lanoue L, Lawson TN, Lek M, Mark M, Marschall S, Mason J, McElwee M, Newbigging S, Nutter LM, Peterson KA, Ramirez-Solis R, Rowland DJ, Ryder E, Samocha KE, Seavitt JR, Selloum M, Szoke-Kovacs Z, Tamura M, Trainor AG, Tudose I, Wakana S, Warren J, Wendling O, West DB, Wong L, Yoshiki A; International Mouse Phenotyping Consortium; Jackson Laboratory; Infrastructure Nationale PHENOMIN, Institut Clinique de la Souris (ICS);

Charles River Laboratories; MRC Harwell; Toronto Centre for Phenogenomics; Wellcome Trust Sanger Institute; RIKEN BioResource Center, MacArthur D, Tocchini-Valentini GP, Gao X, Flicek P, Bradley A, Skarnes WC, Justice MJ, Parkinson HE, Moore M, Wells S, Braun RE, Svenson KL, de Angelis MH, Herault Y, Mohun T, Mallon AM, Henkelman RM, Brown SD, Adams DJ, Lloyd KC, McKerlie C, Beaudet AL, Bućan M, Murray SA, High-throughput discovery of novel developmental phenotypes. Nature 537, 508–514 (2016). [PubMed: 27626380]

81. Sanjana NE, Shalem O, Zhang F, Improved vectors and genome-wide libraries for CRISPR screening. Nat. Methods 11, 783–784 (2014). [PubMed: 25075903]
82. Yu CH, Davidson S, Harapas CR, Hilton JB, Mlodzianoski MJ, Laohamonthonkul P, Louis C, Low RRJ, Moecking J, De Nardo D, Balka KR, Calleja DJ, Moghaddas F, Ni E, McLean CA, Samson AL, Tyebji S, Tonkin CJ, Bye CR, Turner BJ, Pepin G, Gantier MP, Rogers KL, Arthur KM, Crouch PJ, Masters SL, TDP-43 triggers mitochondrial DNA release via mPTP to Activate cGAS/STING in ALS. Cell 183, 636–649.e18 (2020). [PubMed: 33031745]
83. Efthymiou A, Shaltouki A, Steiner JP, Jha B, Heman-Ackah SM, Swistowski A, Zeng X, Rao MS, Malik N, Functional screening assays with neurons generated from pluripotent stem cell-derived neural stem cells. J. Biomol. Screen 19, 32–43 (2014). [PubMed: 24019252]

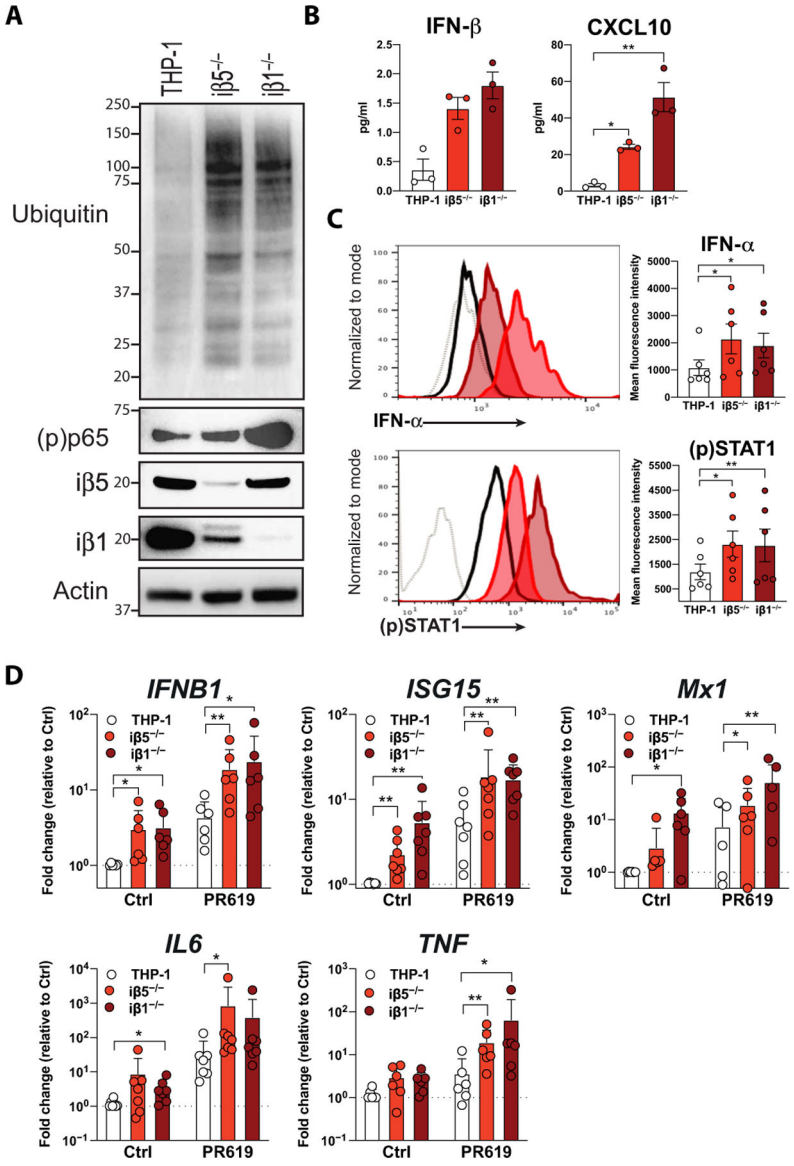

Fig. 1. CRISPR-Cas9–mediated deletion of iβ5 or iβ1 generates cell lines that recapitulate the molecular hallmarks of PRAAS pathology.

CRISPR-Cas9 gene editing was used to delete the inducible proteasome subunit genes *PSMB8* and *PSMB9* from the monocytic cell line, THP-1. (**A**) Accumulation of ubiquitinated proteins and successful deletion of *PSMB8* and *PSMB9* was assessed by immunoblotting for total ubiquitin and the proteasomal subunits iβ5 and iβ1 (encoded for by *PSMB8* and *PSMB9*, respectively). Phosphorylation of p65 in THP-1, iβ5$^{-/-}$, and iβ1$^{-/-}$ cell lines was assessed by immunoblotting with actin used as a loading control. (**B**) Secretion of IFN-β and the IFN inducible chemokine CXCL10 by THP-1, iβ5$^{-/-}$, and iβ1$^{-/-}$ lines were assessed using ELISA. (**C**) Levels of IFN-α and phosphorylated (p)STAT1 in parental THP-1 (black line), iβ5$^{-/-}$ (red), and iβ1$^{-/-}$ (maroon) cell lines were assessed by flow cytometry, gray lines represent unstained cells. Histograms are representative of four independent experiments summarized in column graphs. (**D**) iβ5$^{-/-}$, iβ1$^{-/-}$, and THP-1 cells were treated for 14 hours with the nonspecific DUB inhibitor: PR619 (5 μM) and

expression of stated inflammatory genes were assessed by qPCR. Data are pooled from at least three experiments, and statistical significance was assessed by a ratio paired *t* test, where * indicates $P < 0.05$ and ** indicates $P < 0.01$.

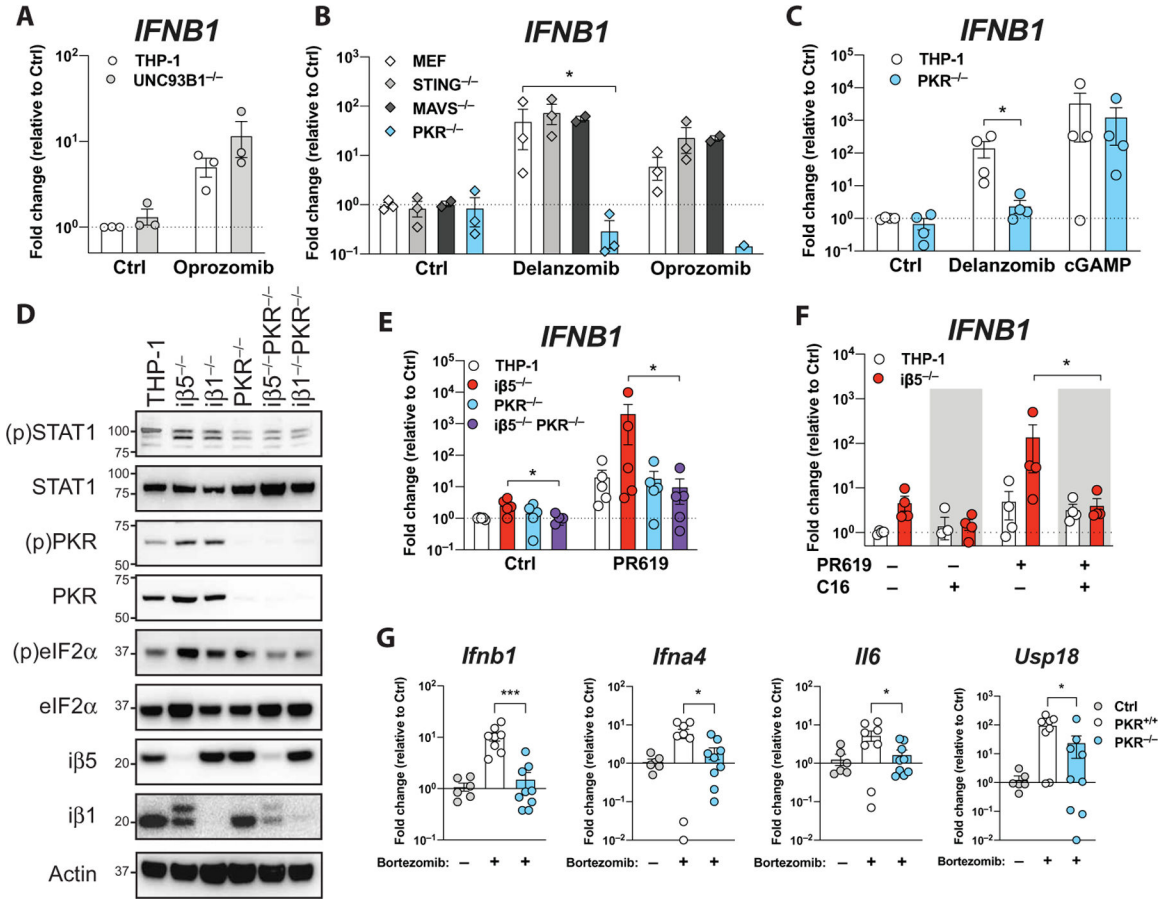

Fig. 2. Proteasome dysfunction–induced inflammation is PKR dependent in vitro and in vivo.

(**A**) CRISPR-Cas9 gene editing was performed on THP-1 cells to generate *UNC93B1* deficient THP-1 cells (UNC93B1$^{-/-}$). Cells were treated with oprozomib (500 nM) for 16 hours, and qPCR was used to assess *IFNB1* gene induction. (**B**) MEF cell lines deficient in *MAVS* (MAVS$^{-/-}$), *TMEM173* (STING$^{-/-}$), and *EIF2AK2* (PKR$^{-/-}$) were treated with delanzomib (200 nM) or oprozomib (500 nM), and *IFNB1* gene induction was assessed by qPCR. (**C**) *EIF2AK2* was CRISPR-Cas9 deleted from THP-1 cells (PKR$^{-/-}$), and cells were treated with delanzomib (200 nM) or the STING agonist: cGAMP (10 μg/ml), as indicated, for 16 hours, and induction of *IFNB1* mRNA was assessed by qPCR. (**D**) *EIF2AK2* was deleted from iβ5$^{-/-}$ and iβ1$^{-/-}$ THP-1 cells to generate PKR$^{-/-}$iβ5$^{-/-}$ and PKR$^{-/-}$iβ1$^{-/-}$ cell lines. Immunoblotting was performed on THP-1, iβ5$^{-/-}$, iβ1$^{-/-}$, PKR$^{-/-}$, PKR$^{-/-}$iβ5$^{-/-}$, and PKR$^{-/-}$iβ1$^{-/-}$ cells to assess phosphorylation (p) of STAT1, PKR, and eIF2α. (**E**) Induction of *IFNB1* mRNA upon PR619 (5 μM) treatment of THP-1, iβ5$^{-/-}$, and PKR$^{-/-}$iβ5$^{-/-}$ cells was assessed by qPCR. (**F**) iβ5$^{-/-}$ or THP-1 cells were cultured with the PKR inhibitor: C16 (0.5 μM) and/or PR619 (5 μM) for 14 hours, induction of *IFNB1* was assessed by qPCR. (**G**) PKR$^{-/-}$ and littermate (PKR$^{+/+}$) mice were treated with bortezomib (1 mg/kg) or vehicle control (Ctrl) for 18 hours. Cardiac bleeds were processed for RNA, and expression of *Ifnb1*, *Ifna4*, *Il6*, and *Usp18* was assessed by qPCR. Data are pooled from at least three experiments, and statistical significance was assessed by ratio paired *t* test for in

vitro experiments and by Student's *t* test for in vivo results. * indicates $P < 0.05$ and *** represents $P < 0.001$.

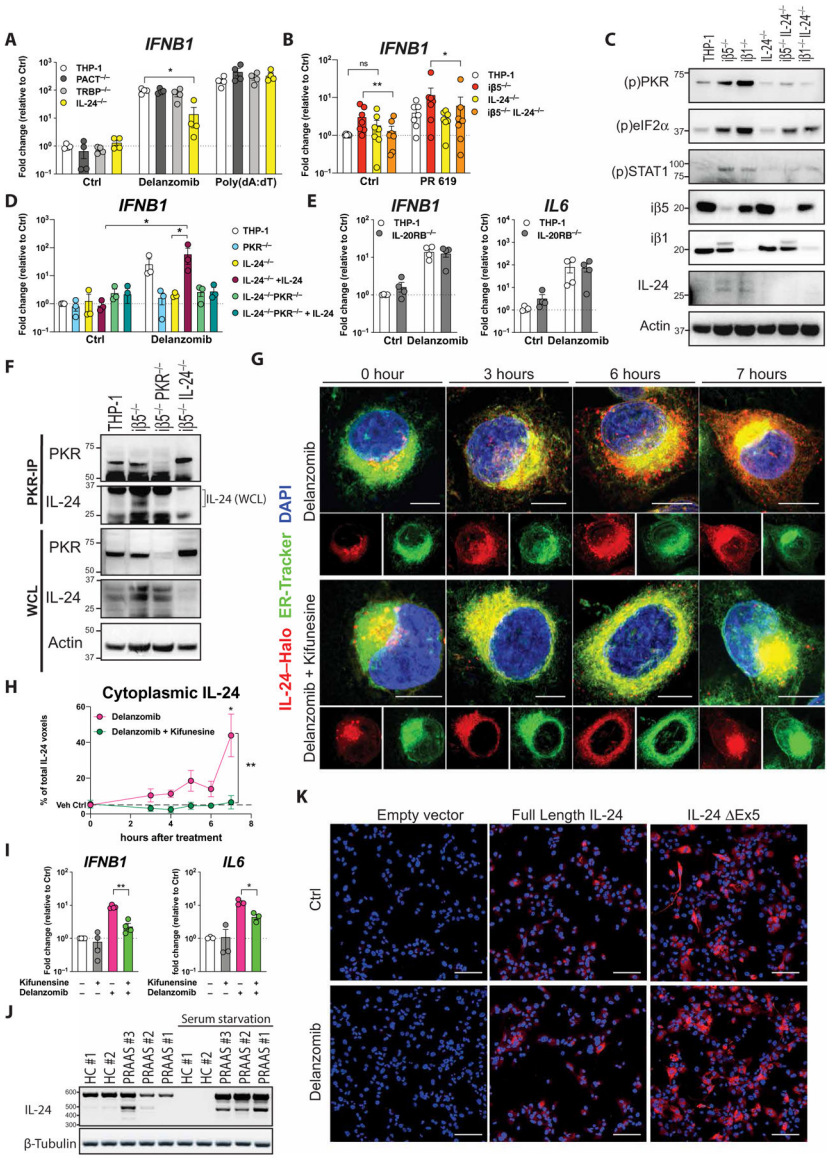

Fig. 3. Cytosolic IL-24 activates PKR to drive inflammatory signaling under conditions of proteasome inhibition.

(**A**) CRISPR-Cas9 gene editing was used to delete *IL24*, *PRKRA*, and *TARBP2* genes in THP-1 cell lines to generate cells deficient in IL-24, PACT, and TRBP (respectively). Cells were then treated for 16 hours with delanzomib (200 nM), poly(dA:dT) (1 μg/ml), or vehicle control (Ctrl) as indicated, and induction of *IFNB1* mRNA was assessed by qPCR. (**B** and **C**) *IL24* was CRISPR- Cas9– deleted from iβ5$^{-/-}$ or iβ1$^{-/-}$ cells, and (B) induction of *IFNB1* mRNA was assessed by qPCR in iβ5$^{-/-}$, IL-24$^{-/-}$, iβ5$^{-/-}$IL-24$^{-/-}$, and parental THP-1 cell lines. (C) Immunoblotting was performed on parental, iβ5$^{-/-}$, and iβ1$^{-/-}$ THP-1 cells sufficient or deficient in IL-24 to assess phosphorylation (p) of STAT1, PKR, and eIF2α. (**D**) IL-24 tagged with HA or empty vector control was stably expressed in IL-24$^{-/-}$ or IL-24$^{-/-}$PKR$^{-/-}$ THP-1 cells by lentiviral transfection. Cells were treated with delanzomib (200 nM) for 16 hours, and induction of *IFNB1* was assessed by qPCR. (**E**) The IL-24 receptor subunit, *IL20RB* was CRISPR-Cas9–deleted from THP-1 cells, cells

were then treated with delanzomib (200 nM) for 16 hours and induction of *IFNB1* was assessed by qPCR. (**F**) PKR-IP and WCLs from THP-1, iβ5$^{-/-}$, iβ5$^{-/-}$PKR$^{-/-}$, and iβ5$^{-/-}$ IL-24$^{-/-}$ cell lines were immunoblotted for PKR, IL-24, and actin (loading control). (**G**) IL-24–Halo was stably expressed in U2OS cells. Super-resolution microscopy was then performed to monitor IL-24–Halo cellular localization during proteasome inhibitor treatment (delanzomib, 200 nM). Egress of IL-24–Halo from the ER to the cytosol could be inhibited by kifunesine. Representative images of specified timepoints are displayed, IL-24–Halo in red, ER-Tracker in green and DAPI in blue. White scale bars, 10 μM. (**H**) Three to seven representative cells from each time point from (G) were analyzed using Imaris software to determine percentage IL-24–Halo outside the ER (cytoplasmic IL-24). (**I**) THP-1 cells were treated with delanzomib (200 nM) and/or kifunesine (50 nM) for 14 hours and induction of *IFNB1* and *IL6* was assessed by qPCR. (**J**) Expression of IL-24 splice isoforms, and β-tubulin mRNA expression was analyzed by PCR in PRAAS patient and HC fibroblast lines, under normal conditions (lanes 1 to 5) and serum starvation (lanes 6 to 10). (**K**) THP-1 cells were stably transfected with HA-tagged full length IL-24 or IL-24 ΔEx5 (as indicated). Differentiation into macrophages was performed using PMA (72 hours), and IF for IL-24 (HA tag) in red and DAPI in blue was assessed at baseline and 14 hours after treatment with delanzomib (200 nM). Data are pooled from three to four experiments, and statistical significance was assessed by ratio paired *t* test, where * indicates $P < 0.05$, ** indicates $P < 0.01$, and ns indicates not significant, with the exception of (H) where statistical significance was assessed by two-way ANOVA with Bonferrioni post tests for individual time points, where ** denotes $P < 0.01$, and * indicates $P < 0.05$.

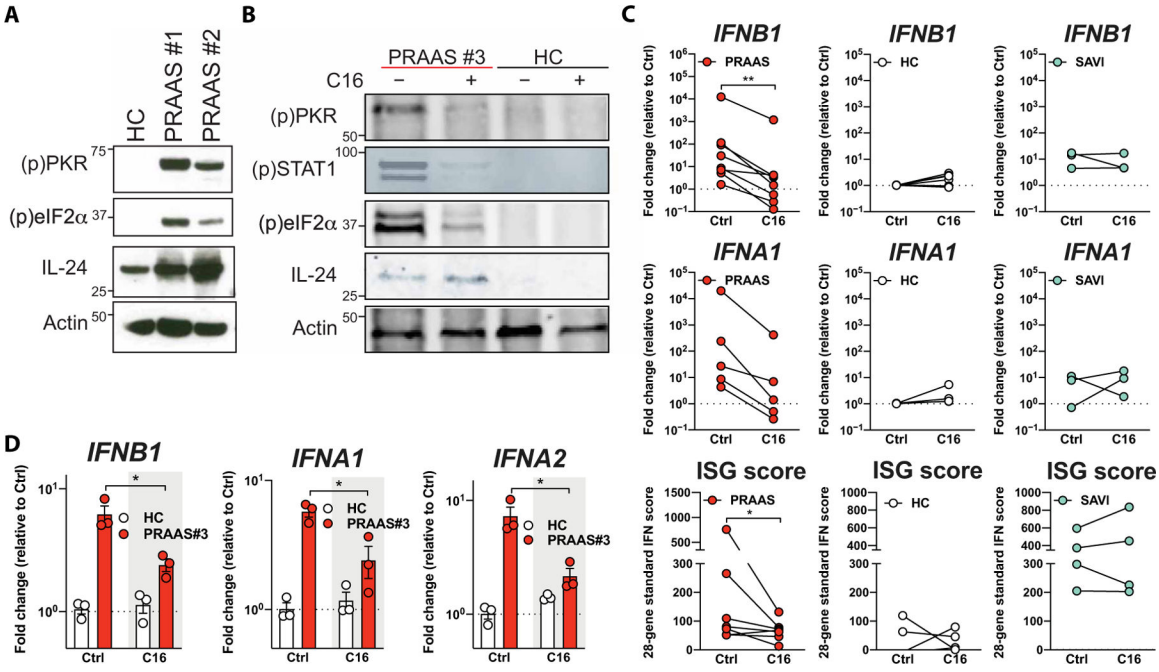

Fig. 4. PKR mediates inflammatory signaling in PRAAS patient samples.

(**A**) Lysates from patient fibroblasts were immunoblotted for (p)PKR and (p)eIF2α, as well as IL-24 and actin. (**B**) Patient PBMCs were treated with C16 (0.5 μM) for 8 hours, and protein lysates were then immunoblotted for (p)PKR, (p)STAT1, and (p)eIF2α, as well as IL-24 and actin. (**C**) PBMC samples from PRAAS and SAVI patients as well as HC samples were cultured with C16 for 8 to 14 hours. Expression of *IFNB1* and *IFNA1* was assessed by qPCR. IFN-αβ induction of ISGs was assessed by NanoString Technologies to generate an ISG score. Significance was assessed by Wilcoxon matched-pair signed-rank test, where * indicates $P < 0.05$ and ** denotes $P < 0.01$. (**D**) iPSC-derived macrophages from PRAAS patient #3 and a HC were assessed for expression of *IFNB1*, *IFNA1*, and *IFNA2* at baseline and after 8 hours of treatment with C16 (1 μM). Significance was assessed by Student's *t* test, * indicates $P < 0.05$.